J. Astrophys. Astr. (2001) **22**, 81–119

Hydrogen Recombination Lines near 327 MHz – II : A Galactic Plane Survey with a $2^\circ \times 6'$ Beam

D. Anish Roshi[1] * & K. R. Anantharamaiah [2]

[1]*National Centre for Radio Astrophysics, TIFR, Pune, India*
[Present Address: National Radio Astronomy Observatory, Green Bank, USA]
[2] *Raman Research Institute, Bangalore-560 080, India.*

Received 2000 October 6; accepted 2000 December 23.

Abstract. In a previous paper we presented a low-resolution ($2^\circ \times 2^\circ$) survey of radio recombination lines (RRLs) at 327 MHz in the longitude range $l = 330^\circ$ to 0° to 89°. In this paper, we present the results of a higher resolution ($2^\circ \times 6'$) survey of RRLs from seven 2°-wide fields and two 6°-wide fields in the same longitude range. Observations were made using the Ooty Radio Telescope (ORT). A total of 252 spectra that were obtained are presented. RRLs were detected in almost all the individual positions within the fields with $l < 35^\circ$ and at several individual positions within the fields in the longitude range $l = 35^\circ$ to 85°. Detailed analysis of the data towards the field centered at G45.5+0.0, shows that the line emission consists of discrete zones of ionized gas. The angular extent of these zones are likely to be one degree or more corresponding to a linear size of > 110 pc at the kinematic distance.

Key words: Galaxy: general – H II regions – ISM: clouds – ISM: general – ISM: structure – radio lines: ISM.

1. Introduction

Radio Recombination Lines (RRLs) are normally observed from compact, dense H II regions that are bright in radio continuum. Several surveys of RRLs at frequencies near 4.8 GHz (Downes *et al.* 1980, Caswell & Haynes 1987), 10 GHz (Lockman 1989) and 15 GHz (Wood & Churchwell 1989) have been made towards discrete H II regions in the Galaxy. The physical properties derived from these observations show that there exists a variety of H II regions. At one extreme are the ultra-compact H II regions with $n_e > 10^4$ cm^{-3} and sizes $\ll 1$ pc which are

*e-mail: aroshi@nrao.edu

formed around young, hot stars (Wood & Churchwell 1989). H II regions with densities between $n_e \sim 50$ and 1000 cm^{-3} and size ranging from few parsecs to few tens of parsecs are widely observed in the Galaxy. These regions have a relatively narrow range of temperatures ($T_e \sim$ 3000–10000 K).

In early observations by Gottesman & Gordon (1970) and Gordon & Cato (1972), at frequencies < few GHz, RRLs were detected from several positions along the galactic plane which are free of discrete continuum sources. These low frequency RRLs do not originate in compact, dense H II regions due to the effects of continuum opacity, pressure broadening and beam dilution (Shaver 1975). These RRLs originate from low-density ionized gas ($n_e \sim 0.5 - 50$ cm^{-3}). Several surveys of RRLs near 1.4 GHz have been made (Hart & Pedlar 1976, Lockman 1976, 1980, Cersosimo 1990, Heiles, Reach & Koo 1996) to study this component of the Galaxy. RRLs from this gas were also observed by Anantharamaiah (1985a) near 325 MHz. These observations were used to study the distribution and physical properties of the low-density ionized gas (Hart & Pedlar 1976, Lockman 1976, 1980, Anantharamaiah 1985b, 1986) and also its association with other components of the Galaxy. Several suggestions have been made on the origin of this low-density ionized gas. Matthews, Pedlar & Davies (1973) and Shaver (1976) suggested that the low-density component is a population of "evolved H II regions". Mezger (1978) portrayed this gas as an ensemble of low-density H II regions which he referred to as "extended low-density" (ELD) ionized gas. Heiles *et al.* (1996) suggested a morphological model where the ELD gas is conflated with the "Warm Ionized Medium" and referred to it as "extended low-density warm ionized medium" (ELDWIM) (Petuchowski & Bennett 1993, Heiles 1994, Heiles *et al.*1996). Anantharamaiah (1986) suggested that the low-density ionized gas are associated with large, low-density envelopes of normal H II regions.

In a previous paper, Roshi & Anantharamaiah (2000) (hereafter paper I) presented a new, extensive low-resolution ($\sim 2^\circ \times 2^\circ$) observations of RRLs near 327 MHz from the Galactic plane. A part of the Ooty Radio Telescope (ORT) with a size of 23 m × 23 m, called a 'module', was used for these observations. RRLs were detected in more than 80 % of the observed positions in the longitude range l = 332° to 0° to 89° (inner Galaxy). The observed RRL emission showed large fluctuations as a function of galactic longitude indicating that the line emitting region may be clumpy (paper I). Higher resolution observations can help in studying the nature of the clumpiness and in determining the angular size of the line emitting region. With these objectives in mind, we observed a selected set of 2°-wide fields in the inner Galaxy using the full ORT (530m × 30 m) which gives a beam of 2° × 6′. This paper discusses these higher resolution observations and is organized as follows. The observations and results are described in Section 2. Comparison of the average spectra over a 2° × 2° region and the spectra obtained in the same direction in the low resolution survey is made in Section 3. Section 4 discusses the angular extent of the line emitting region inferred from the higher resolution observations. The paper is summarized in Section 5.

2. Observations and Results

The RRL survey was made using the ORT which is a 530 m x 30 m parabolic cylinder operating at a nominal center frequency of 327 MHz (Swarup *et al.* 1971). In the normal configuration of the ORT, the signals received by groups of 48 dipoles of the 1056 element linear array at the focal line are added in phase. 22 such groups, which are known as "modules", each having a half power beam width of $2^\circ.3$ (in RA) $\times$ $2^\circ.2$ sec(δ) (in Dec.), are combined later through a beam forming network to produce twelve beams of $\sim 2^\circ \times 5'.5 \sec(\delta)$, δ being the declination. The twelve beams are spread along the north-south direction separated by $3' \sec(\delta)$. The spectrometer used for the observations was configured (see below) to collect data from two such beams simultaneously. The two selected beams are separated in the sky by $6' \sec(\delta)$.

The center frequency of operation of the ORT is 326.5 MHz. The RRL transitions from principal quantum numbers n = 270, 271, 272 and 273 with $\Delta n = 1$ fall inside the 15 MHz bandwidth of the ORT. A digital spectrometer which could simultaneously observe all the four transitions with a velocity resolution of $\sim$ 1.0 km s^{-1} (Paper I) was used. The four RRL transitions from two beams were observed simultaneously using 2 such spectrometers. The reference spectrum was obtained by switching the frequency every second by half the bandwidth (i.e. 384 KHz). The velocity coverage is about 320 km s^{-1} after rejecting the edge channels. The final spectrum is obtained by averaging the four spectra corresponding to the four RRL transitions of each beam. Thus two final spectra from two sky positions, separated in declination by $6' \sec(\delta)$, are obtained from each observing session. Details of the mode of observations and the data reduction procedure have been presented in paper I.

RRL at low frequencies are weak (line to system temperature ratio $\sim 10^{-3}$) and hence it is extremely time consuming to make a complete survey of the galactic plane with the $2^\circ \times 6'$ beam. Therefore we selected a set of seven fields which are 2° wide and two fields which are 6° wide in longitude. The selected fields were spread over the longitude range $l = 347^\circ$ to 0° to 67°. Fig. 1 (Appendix 2 contains all the figures of this paper) shows schematically all the positions in the galactic plane observed with the $2^\circ \times 6'$ beam. Except for the two 6°-wide fields, the beam centers were chosen so that a set of 20 adjacent positions in declination correspond to a $2^\circ \times 2^\circ$ region from which RRLs were observed in the low-resolution survey (paper I). For the two 6°-wide fields, the center of the two beams of the ORT, from which RRLs were observed simultaneously, is positioned at the galactic plane. Since the ORT is a north-south oriented telescope, the $2^\circ \times 2^\circ$ beam is inclined with respect to the galactic plane. Figs. 2 to 15 (Appendix 2) present all the observed spectra. In these figures, spectra are grouped such that they correspond, wherever possible, to a $2^\circ \times 2^\circ$ field observed at lower resolution using a single 'module' of the ORT (see paper I). A contour map of the 11 cm continuum emission (Reich *et al.* 1990) towards the $2^\circ \times 2^\circ$ field is also shown in each figure to compare the continuum emission within the observed fields. For example, field 9

is devoid of any bright, extended continuum emission (see Fig. 15). An average of all the individual spectra within the 2° field and the corresponding lower resolution spectrum (taken from paper I) are also given in each of these figures. The average spectrum, obtained from the 20 adjacent higher resolution observations should be equivalent to the spectrum observed in the low resolution survey towards the same direction (see Section 3). Table 1 (Appendix 1 contains all the Tables of this paper) gives a summary of the observations and the parameters derived from the line profiles shown in Figs. 2 to 15 in Appendix 2. The observed spectra are given in units of T_L/T_{sys}, where T_L is the line antenna temperature and T_{sys} is the system temperature. The velocity resolution to which the final spectra (shown in Figs. 2 to 15) are smoothed is given in column 6 of Table 1. Effective integration time for the spectra range from 8 hrs to 12 hrs. In many of the spectra, two emission features are detected. The feature at the higher velocity is the hydrogen line and the feature which is about -150 km s^{-1} from the hydrogen line is most likely a carbon recombination line. In many cases, the detected carbon lines are almost as strong as the hydrogen line in spite of the small C/H abundance ratio in the ISM ($< 3 \times 10^{-4}$) indicating that the two lines arise in regions with different physical properties. The carbon lines seen in Figs 2 to 15 most likely belong to the class of low-frequency recombination lines first observed in absorption at 26 MHz by Konovalenko & Sodin (1980). These RRLs were shown to turn over into emission above 200 MHz (Payne, Anantharamaiah & Erickson 1989) and to be widespread in the inner Galaxy (Erickson, McConnell & Anantharamaiah 1995, Kantharia & Anantharamaiah 2001). Carbon RRLs are not discussed further in this paper.

Hydrogen lines were detected in almost all the positions in the fields with $l < 35°$. In several cases, the line parameters seem to vary when the beam center is moved by $6'$ in declination. For example, the width of the lines detected towards G347.78−0.14 and G347.70−0.20 differ by more than a factor of two. These two positions are separated in declination by only 0°.1. The range in the central velocity of the lines observed towards fields with $l < 35°$ is typically 15 km s^{-1}. This difference is about half the typical line width observed in the survey. RRLs were not detected in many positions within the fields with $l > 35°$ (Figs 11 to 15 in Appendix 2).

2.1 *Line widths*

The width of the RRLs detected in these observations are in the range 20 – 45 km s^{-1}. Fig. 16 (Appendix 2) shows the histogram of the observed line widths. The median line width is 32.5 km s^{-1} which is somewhat large compared to the width of lines from normal H II regions ($\sim$ 26 km s^{-1}; Lockman *et al.* 1996). Line widths near 327 MHz can be affected by pressure broadening (Shaver 1975) and blending of lines from objects within the beam or from objects along the line of sight with different central velocities. In a few positions, the line width observed is less than 10 km s^{-1}, which constrains the kinetic temperature of the line emitting region to < 2200 K.

Comparison of the distribution of line widths obtained from the observations with $2^\circ \times 2^\circ$ (paper I) and $2^\circ \times 6'$ beams shows that they are similar. The median widths from the low resolution observations is ~ 31 km s^{-1} (paper I). If the broadening is due to blending of lines from different objects either along the line of sight or within the beam, then we may expect larger widths in the low resolution survey. However, the low resolution observations are not sensitive to line emitting zones of relatively small angular extent due to beam dilution. On the other hand, such line emitting zones can contribute to line emission observed with the $2^\circ \times 6'$ beam. Thus it is possible for the lines detected in the two observations to have similar median widths. Examination of the distribution of the widths, obtained from the two observations, shows that lines with width between 50 and 70 km s^{-1} are observed more frequently in the low resolution survey. These larger widths are most likely due to blending of lines from different objects within the coarse beam. Towards a few positions (e.g. G6.11+0.03), line with widths ~ 10 km s^{-1} has been observed in the high resolution survey. Such narrow lines are not detected in any of the positions in the $2^\circ \times 2^\circ$ observations.

2.2 l-v *Diagram*

An *l-v* diagram obtained from the data in Table 1 is shown in Fig. 17 (Appendix 2). Some confinement of line emission to the spiral arms 2 and 3 below $l = 50^\circ$ is seen in the *l-v* diagram. On the other hand, at longitudes $l > 50^\circ$, the line emission does not seem to be confined to any of the spiral arms. The *l-v* diagram shows good similarity with that obtained by Anantharamaiah (1985a) from the H272α line observations with similar resolution towards a selected set of sources in the longitude range $-2^\circ < l < 50^\circ$. The concentration of line emission towards galactocentric radius of ~ 5.0 kpc near longitude 15° and the extension of emission to negative velocities in the longitude range $l < 10^\circ$ are evident in both the *l-v* diagrams. The *l-v* diagram obtained from the present observations shows, in general, good similarity with that obtained from the low resolution ($2^\circ \times 2^\circ$) survey (paper I). The line emission observed in the higher resolution survey at longitude $l > 50^\circ$ shows extension towards the negative velocities in the *l-v* space which is not observed in the low resolution survey.

3. Comparison with the low resolution observations

With the higher resolution beam ($2^\circ \times 6'$) used in these observations, 20 independent positions can be observed within the $2^\circ \times 2^\circ$ beam of the lower resolution survey presented in paper I. The higher resolution observations are therefore grouped into sets of 20 spectra. The aim is to average the 20 spectra in each of these sets and compare it with the spectrum obtained with the low resolution beam in the same direction and also to examine all the spectra within a 2° field for possible variations.

The average spectrum, obtained from the the 20 adjacent high resolution beam observations, should be equivalent to the spectrum observed in the low resolution

survey towards the same direction. The signal to noise ratio (SNR) of the two spectra will differ by the square root of the ratio of the total integration times involved. Two effects which can make the average spectrum different from the spectrum obtained in the low resolution survey in the same direction; (a) the 20 spectra are averaged without taking into account the angular response function of the low resolution beam, and (b) the integration time at different positions in the high resolution observation and the system temperature at different positions within the low resolution beam are not the same. The spectrum obtained by averaging the 20 spectra towards a given $2^\circ \times 2^\circ$ region and that observed in the same direction in the low resolution survey are also shown in Figs. 2 to 15. Table 2 (Appendix 1) gives the line parameters (columns 3,4,5) obtained from these spectra along with the spectral resolution (column 6) and the effective integration time (column 8). Examination of Table 2 shows that the parameters of the hydrogen line in the average spectrum in most of the fields agree, within the signal to noise ratio, with those of the spectrum obtained in the low resolution survey. In fields 1 and 8, the line width observed in the low resolution survey and that obtained from the average spectrum are different. The line emission appears to be complex in the field 6c, which makes it difficult to fit a proper baseline to the spectrum. A larger bandwidth is required for observation in this direction, since line emission seems to extend over a large velocity range.

In two fields, 6a and 9 (Figs. 10 & 15), the line structure in the average spectrum is different from that of the corresponding spectrum from the low resolution survey. The average spectrum towards field 6a consists of two hydrogen line features. The line feature with central velocity close to that observed in the low resolution survey has line width $\sim$ 30 km s^{-1} which is larger than the width of the line ($\sim$ 14 km s^{-1}) observed with the $2^\circ \times 2^\circ$ beam. If we assume that the line intensities (in units of T_L/T_{sys}) in the average spectrum and the spectrum obtained with the $2^\circ \times 2^\circ$ beam are similar, then the line features seen in the average spectrum should be at about the 2σ level in the spectrum obtained in the low resolution survey. Towards field 9, no line emission is detected in the low resolution survey whereas a line feature is detected (see Table 2) in the average spectrum. The line feature seen in the average spectrum should have been detected at $> 3\sigma$ level in the spectrum obtained in the low resolution survey if we assume that the line intensities in both spectra are similar. While the observations towards field 6a may be consistent within the signal to noise ratio, further investigation is required to understand the discrepancy observed towards field 9.

4. Angular extent of the line emitting region

In this section we will try to answer the question "do the RRL emitting regions consist of ionized clumps with emission confined to small angular regions or is the emission extended and uniform over a large area ? " The higher resolution observations show different behavior of line emission for $l < 35^\circ$ and for $l > 35^\circ$. While RRLs were detected in almost all the individual positions within the fields

with $l < 35°$, lines were not detected in several individual positions within the fields in the longitude range $l = 35°$ to $85°$.

If the line emission originates from a homogeneous, ionized region with angular extent of several degrees, then the line parameters observed at positions within this angular span are expected to be similar. Examination of the observed spectra shows that at several positions there is a considerable change in the line parameters when the beam center is moved by even $6'$ in declination. For example, towards the position G4.72+0.02, the detected line has a width of 49 km s^{-1} and a central velocity of ~ 2 km s^{-1} while the line parameters at G4.64−0.03 are $\Delta V = 27$ km s^{-1} and $V_{LSR} \sim 8$ km s^{-1}. The beam centers of these two positions differ by $0°.1$. This difference implies that the line emitting zones have structures on an angular scale of $\sim 0°.1$, which is ~ 10 pc, if the distance to the source producing the line emission is 5 kpc. This scale is smaller than the typical size of the line emitting regions estimated in Roshi & Anantharamaiah (2001). It seems that the line emission in fields with $l < 35°$ originate from ionized regions which may extend over several degrees but which may have clumps with angular structures as small as $0°.1$.

4.1 *Line emission towards the field G45.5+0.0*

We present a more detailed analysis of one of the observed fields, G45.5+0.0 (Fig. 13). The line of sight through the galactic disk over an angle of $2°$ towards G45.5+0.0 is shown in Fig. 18 (Appendix 2). The line-of-sight intersects the spiral arm 4 at one position and arm 3 at two places. The distances to the three regions of intersection are ~ 4.7 kpc, 7.8 kpc and 10.7 kpc. The expected radial velocities for these distances are 58, 56 and 17 km s^{-1} respectively. H II regions identified from higher frequency RRL observations in this field are listed in Table 3 (Appendix 1) along with the line parameters. RRL near 327 MHz is detected towards some of these positions and their parameters are also given in Table 3. The central velocities of the 327 MHz lines and those detected from H II regions at higher frequencies are comparable.

Examination of the 20 spectra obtained from this field (Fig. 13) shows unambiguous presence of lines in only 3 positions. If the line emission is confined to only these 3 positions, then the expected SNR of the spectrum obtained by averaging 20 spectra is 2.2. However the actual SNR of the line in the average spectrum is 5.9. This increased SNR clearly indicates that the line emission is not confined to only 3 positions but spread over a good fraction of the $2°$ region. To determine the actual angular extent of the line emission, the following analysis was made. Different subsets of the 20 spectra were averaged as shown in Fig. 19 (Appendix 2). The spectra in the left column are obtained by averaging the spectra at adjacent positions. Thus they are equivalent to observing with a beam of $2° \times 12'$. The spectra in the central column, obtained by averaging five adjacent spectra, have an effective beam of $2° \times 0°.5$. The rightmost column shows spectra with an effective beam of $2° \times 1°$. Line parameters of all possible emission features in these spectra are derived and tabulated in Table 4 (Appendix 1). A narrow (~ 11 km s^{-1}) feature appears

to be present in all the spectra in the longitude range G44.67−0.4 to G45.47−0.0 (Fig. 19). This feature does not seem to be present either in other individual spectra or in the spectrum averaged over 1° centered at G45.95+0.2 (see Fig. 19). Thus the region responsible for this line is less than 1° in extent. The central velocity of line emission indicates a kinematic distance to the line emitting region of 6.3 kpc and the estimated size of the region is $\sim$ 110 pc. The individual spectra towards the positions G46.35+0.4 to G45.56+0.0 of field 7 (see Table 1) do not seem to have a common component, although the integrated spectrum obtained by averaging them to an effective beam of 2° × 1° shows a broad feature ($\sim$ 35 km s^{-1}). Such broad features are also present in the spectra obtained by averaging over a 2° × 12′ region centered on G46.30+0.43 and G45.6+0.05 (see Fig. 19). These regions contain known H II regions. The 2.7 GHz continuum emission from the H II region G46.495−0.247 overlaps with the 2° × 12′ region centered on G46.30+0.43 (see Fig. 13). The 2° × 12′ region centered on G45.60+0.05 contains the H II regions G45.475+0.13 and G45.451+0.06. The central velocities of the features seen in the integrated spectra towards G46.30+0.43 and G45.60+0.05 are comparable with those obtained from the H II regions. We thus conclude that the line emission towards the field G45.5+0.0 consists discrete emission zones. Some of the discrete zones have an angular size as large as a degree or more. There is some evidence for the line emission zones to be associated with the H II regions in the field. Similar analysis of other fields (Figs. 2 to 15) will be presented elsewhere.

5. Summary

In an earlier paper (paper I) we presented a low-resolution (2° × 2°) survey of RRLs at 327 MHz in the inner Galaxy made using a single module of the ORT. In this paper, we discussed RRL observations at 327 MHz with the full ORT (i.e. all 22 modules), which gives an angular resolution of 2° × 6′. These observations are used to understand the spatial structure of the line emission observed in the low resolution survey. Seven 2°- wide fields and two 6°- wide fields in the inner Galaxy were observed with the 2° × 6′ beam. A total of 252 spectra were obtained from the higher resolution observations. RRLs were detected in almost all individual positions within the fields with $l < 35°$ and at several individual positions within the fields in the longitude range $l = 35°$ to 85°. The line width observed in these observations were in the range 20 km s^{-1} to 40 km s^{-1}. In most cases, the integrated spectrum obtained by averaging the 20 higher resolution spectra towards a 2° × 2° region is similar, to the spectrum observed at low resolution. Analysis of the line emission in the high resolution observations towards fields with $l < 35°$ indicates that the line emitting region is extended over several degrees but is clumpy. The clump size can be $\sim$ 10 pc or less. A more detailed analysis of the data towards one of the fields, G45.5+0.0, shows that the line emission consists of discrete zones of ionized regions. The angular extent of these zones are likely to be one degree or more corresponding to linear sizes of > 110 pc at the kinematic distance obtained

from the central velocity of line emission. There is some evidence for the line emitting zones being associated with the H II regions in this field.

Acknowledgements

We are grateful to the technical and telescope operation staff at the Radio Astronomy Centre, Ooty, for generous help in conducting the long observations. DAR thanks the Raman Research Institute for generously allowing the use of their research facility. It is a pleasure to acknowledge V. Balasubramanian, A. Pramesh Rao and Jayaram N. Chengalur for many discussions and helpful suggestions. This work forms a part of the Ph.D. thesis of DAR.

APPENDIX 1.

Table 1. Summary of observations with the $2^\circ \times 6'$ beam.

l (^{o})	b (^{o})	T_L/T_{sys} $\times 10^3$	ΔV (km s^{-1})	$V_{\rm LSR}$ (km s^{-1})	V_{res} (km s^{-1})	RMS[1] $\times 10^3$	t_{int} (hrs)
Field 1 (G348.0+0.0)(see Fig. 2 for spectra)							
347.22	−0.56				8	0.14	6.9
347.30	−0.50				5	0.19	7.1
347.38	−0.44	0.55(0.02)	31.4(1.5)	−9.8(0.6)	8	0.15	8.1
347.46	−0.38	0.47(0.02)	39.4(2.3)	−16.1(1.0)	8	0.12	13.8
347.54	−0.32	0.50(0.03)	22.0(1.5)	−11.5(0.6)	5	0.14	12.2
347.62	−0.26	0.58(0.05)	29.3(2.7)	−11.7(1.1)	5	0.16	12.5
347.70	−0.20	0.61(0.03)	11.0(0.7)	−11.7(0.3)	5	0.13	14.2
347.78	−0.14	0.53(0.01)	37.5(1.1)	−13.3(0.5)	8	0.10	16.3
347.86	−0.08	0.52(0.02)	33.3(1.4)	−1.4(0.6)	8	0.12	9.5
347.94	−0.02	0.61(0.03)	35.7(2.2)	−13.1(0.9)	8	0.17	6.9
348.02	+0.03	0.48(0.02)	46.1(2.2)	−15.6(0.9)	8	0.14	10.3
348.10	+0.09	0.63(0.02)	31.0(1.1)	−14.5(0.4)	8	0.10	13.6
348.18	+0.15	0.64(0.02)	39.7(1.5)	−15.4(0.6)	8	0.13	10.7
348.26	+0.21	0.62(0.02)	29.6(0.9)	−19.0(0.4)	8	0.13	15.0
348.42	+0.33				8	0.24	11.3
348.51	+0.39	0.63(0.03)	34.9(2.0)	−18.1(0.8)	8	0.12	13.2
348.67	+0.51	0.55(0.02)	32.4(1.6)	−18.3(0.7)	8	0.14	9.7
348.75	+0.57	0.72(0.03)	31.8(1.5)	−16.1(0.6)	8	0.13	11.5
Field 2a (see Fig. 3 for spectra)							
0.43	−0.02	0.84(0.03)	40.8(1.8)	3.3(0.8)	8	0.17	10.2
0.52	+0.03	0.64(0.02)	44.2(1.6)	−2.3(0.7)	8	0.11	12.8
0.67	−0.00	0.53(0.02)	33.1(1.7)	4.8(0.7)	8	0.11	11.2
0.75	+0.05	0.77(0.04)	34.0(1.9)	0.2(0.8)	8	0.14	11.6
0.84	+0.10	0.72(0.02)	22.4(0.9)	4.5(0.4)	8	0.11	9.4
0.92	+0.16	0.78(0.03)	23.7(1.0)	5.1(0.4)	8	0.11	12.6
Field 2b (G2.3+0.0) (see Fig. 4 for spectra)							
1.12	+0.02	0.52(0.02)	40.4(1.6)	0.4(0.7)	8	0.13	10.2
1.21	+0.07	0.58(0.02)	45.9(1.9)	−4.3(0.8)	8	0.10	10.3
1.29	+0.13	0.40(0.02)	42.8(3.0)	−0.3(1.2)	8	0.12	9.9
1.38	+0.18	0.52(0.02)	41.9(2.1)	5.4(0.9)	8	0.12	10.1
1.58	+0.04	0.66(0.02)	28.3(1.3)	2.1(0.5)	8	0.13	11.8
1.66	+0.09	0.48(0.02)	37.8(2.3)	6.5(0.9)	8	0.12	12.2
1.75	+0.14	0.33(0.03)*	25.9(2.5)	3.2(1.1)	8	0.13	11.1
1.83	+0.20	0.51(0.03)	36.1(2.2)	7.8(0.9)	8	0.13	11.3
2.03	+0.06	0.57(0.02)	28.4(1.2)	1.0(0.5)	8	0.13	12.0
2.12	+0.11	0.46(0.03)	21.9(1.6)	3.6(0.7)	8	0.13	12.4
2.21	+0.16	0.43(0.02)	31.9(2.2)	1.2(0.9)	8	0.11	14.8

Table 1. (*Continued*).

l (°)	b (°)	T_L/T_{sys} × 10^3	ΔV (km s^{-1})	$V_{\rm LSR}$ (km s^{-1})	V_{res} (km s^{-1})	RMS[1] × 10^3	t_{int} (hrs)
2.29	+0.21	0.57(0.02)	21.0(1.4)	11.9(0.6)	8	0.10	14.9
2.54	−0.03				8	0.18	8.1
2.63	+0.02	0.44(0.02)	42.2(2.3)	6.9(1.0)	8	0.11	11.2
2.78	−0.03	0.64(0.02)	34.7(1.2)	7.8(0.5)	8	0.09	11.2
2.86	+0.02	0.44(0.02)	28.2(1.8)	8.5(0.8)	8	0.11	12.5
3.01	−0.03	0.65(0.03)	27.5(1.4)	5.2(0.6)	8	0.12	11.2
3.09	+0.02	0.40(0.03)*	21.4(1.8)	7.2(0.8)	8	0.11	11.7
3.24	−0.03	0.46(0.01)	34.5(1.3)	5.9(0.5)	8	0.15	10.1
3.33	+0.02	0.40(0.02)	26.7(2.0)	8.6(0.8)	8	0.11	11.5
Field 2c (G4.7+0.0) (see Fig. 5 for spectra)							
3.47	−0.03	0.36(0.02)*	33.6(2.4)	7.9(1.0)	8	0.13	9.2
3.56	+0.02	0.57(0.02)	24.7(0.9)	12.5(0.4)	8	0.09	10.4
3.71	−0.03	0.69(0.03)	27.0(1.3)	8.4(0.5)	8	0.14	8.8
3.79	+0.02	0.49(0.02)	34.4(2.0)	4.0(0.8)	8	0.12	11.6
3.94	−0.03	0.66(0.04)	18.3(1.4)	7.3(0.6)	6	0.15	8.4
4.03	+0.02	0.47(0.02)*	25.7(1.5)	11.0(0.6)	8	0.15	11.0
4.17	−0.03	0.47(0.02)	37.9(2.4)	8.6(0.9)	8	0.14	9.2
4.26	+0.02	0.45(0.03)	24.4(1.7)	11.9(0.7)	8	0.11	12.2
4.49	+0.02	0.55(0.04)	15.5(1.1)	9.1(0.5)	6	0.11	11.6
4.64	−0.03	0.45(0.02)	26.6(1.6)	8.4(0.7)	8	0.11	9.6
4.72	+0.02	0.62(0.02)	49.0(1.6)	1.8(0.7)	8	0.12	11.5
4.87	−0.03	0.72(0.04)	28.4(1.7)	8.0(0.7)	5	0.17	8.3
4.95	+0.02	0.49(0.02)	29.1(1.7)	12.4(0.7)	8	0.13	8.5
5.10	−0.03	0.54(0.02)	48.2(2.3)	10.6(1.0)	6	0.16	8.5
5.19	+0.02	0.81(0.02)	35.1(1.1)	9.4(0.5)	6	0.11	9.0
5.33	−0.03	0.61(0.02)	24.4(1.0)	12.2(0.4)	8	0.10	10.2
5.42	+0.02	0.59(0.04)	20.3(1.4)	12.1(0.6)	5	0.14	10.6
5.56	−0.03	0.59(0.03)	44.5(2.3)	8.9(0.9)	8	0.14	10.0
5.65	+0.02	0.69(0.03)	23.2(1.0)	11.2(0.4)	8	0.10	12.3
Field 2d (see Fig. 6 for spectra)							
5.80	−0.03	0.75(0.04)	22.8(1.3)	10.3(0.6)	6	0.16	7.4
5.88	+0.02	0.85(0.03)	30.9(1.1)	10.6(0.5)	8	0.13	8.6
6.02	−0.02	0.75(0.04)	25.0(1.5)	13.1(0.6)	8	0.16	4.2
6.11	+0.03	0.89(0.06)	9.6(0.8)	23.4(0.3)	6	0.18	4.2
6.25	−0.02	0.70(0.03)	30.8(1.8)	16.4(0.7)	6	0.16	5.6
6.34	+0.03	0.86(0.05)	29.4(1.9)	16.3(0.8)	5	0.22	5.6
6.48	−0.02	0.79(0.03)	29.0(1.3)	15.1(0.6)	8	0.15	8.0
6.57	+0.03	1.11(0.06)*	8.4(0.6)	6.6(0.2)	3	0.22	6.8
6.72	−0.02	1.02(0.03)	24.1(0.9)	14.5(0.4)	5	0.14	10.0
6.80	+0.03	0.94(0.02)	28.0(0.9)	15.4(0.4)	5	0.12	11.4

Table 1. *(Continued).*

l (°)	b (°)	T_L/T_{sys} $\times 10^3$	ΔV (km s^{-1})	$V_{\rm LSR}$ (km s^{-1})	V_{res} (km s^{-1})	RMS[1] $\times 10^3$	t_{int} (hrs)
Field 3 (G13.9+0.0) (see Fig. 7 for spectra)							
13.04	−0.46	0.77(0.03)	31.8(1.2)	26.0(0.5)	8	0.13	7.9
13.13	−0.41	0.41(0.02)	43.3(3.0)	28.7(1.2)	8	0.13	10.6
13.22	−0.36	0.61(0.03)	39.5(2.5)	26.0(1.1)	6	0.17	8.2
13.30	−0.36				6	0.18	8.4
13.39	−0.26	0.80(0.03)	39.4(1.7)	27.4(0.7)	8	0.14	8.4
13.48	−0.22	0.76(0.01)	34.3(0.8)	24.9(0.3)	6	0.12	11.2
13.57	−0.17	1.01(0.03)	40.9(1.4)	29.2(0.6)	5	0.16	9.3
13.65	−0.12	0.85(0.03)	32.5(1.3)	26.9(0.6)	6	0.14	9.1
13.74	−0.07	0.90(0.03)	31.5(1.3)	25.9(0.5)	8	0.18	8.0
13.83	−0.02	1.00(0.03)	38.3(1.5)	30.4(0.6)	5	0.21	8.8
13.92	+0.03	1.15(0.03)	48.4(1.4)	33.4(0.6)	8	0.19	6.3
14.00	+0.07	1.10(0.03)	27.1(0.8)	26.2(0.3)	6	0.17	6.7
14.09	+0.12	0.94(0.03)	30.3(1.1)	24.7(0.5)	5	0.15	10.0
14.18	+0.17	0.83(0.02)	40.2(1.4)	24.5(0.6)	6	0.13	10.9
14.27	+0.22	0.80(0.02)	36.6(1.0)	30.4(0.4)	8	0.13	9.9
14.36	+0.26	0.82(0.02)	38.4(1.4)	30.0(0.6)	5	0.13	11.7
14.44	+0.31	0.68(0.03)	26.3(1.4)	25.1(0.6)	8	0.14	7.5
14.53	+0.36	0.63(0.02)	34.9(1.3)	29.8(0.5)	8	0.13	8.0
14.62	+0.41	0.63(0.02)	34.8(1.4)	28.6(0.6)	8	0.14	10.1
14.71	+0.46	0.76(0.03)	22.6(0.9)	25.0(0.4)	6	0.11	11.8
Field 4 (G25.2+0.0) (see Fig. 8 for spectra)							
24.37	−0.44				8	0.13	10.2
24.46	−0.39	0.46(0.03)	19.1(1.3)	104.3(0.5)	8	0.10	10.6
24.55	−0.35				8	0.16	8.4
24.64	−0.30				8	0.14	9.3
24.73	−0.25	0.47(0.03)*	37.0(2.6)	107.2(1.0)	8	0.17	10.4
24.81	−0.21				8	0.16	8.3
24.90	−0.16	0.33(0.02)	61.1(4.7)	95.3(1.6)	8	0.13	14.3
24.99	−0.12				8	0.10	13.9
25.08	−0.07				8	0.15	8.4
25.17	−0.02				5	0.16	10.2
25.26	+0.03				8	0.13	12.4
25.35	+0.07				8	0.12	13.2
25.43	+0.12				8	0.14	10.7
25.52	+0.16				8	0.13	10.9
25.61	+0.21				8	0.13	9.5
25.70	+0.26				8	0.15	9.5
25.79	+0.30	0.55(0.02)	38.6(1.6)	110.6(0.7)	8	0.14	7.2
25.88	+0.35	0.56(0.02)	23.3(0.8)	102.1(0.4)	8	0.12	9.7
25.96	+0.40	0.57(0.03)	16.0(0.9)	99.4(0.4)	8	0.11	8.2
26.05	+0.44	0.47(0.03)	22.2(1.9)	103.2(0.8)	8	0.13	10.6

Table 1. (*Continued*).

l (°)	b (°)	T_L/T_{sys} × 10^3	ΔV (km s^{-1})	$V_{\rm LSR}$ (km s^{-1})	V_{res} (km s^{-1})	RMS[1] × 10^3	t_{int} (hrs)
Field 5 (G27.5+0.0) (see Fig. 9 for spectra)							
26.62	−0.43	0.63(0.01)	33.1(0.8)	95.9(0.3)	8	0.13	7.1
26.71	−0.39	0.35(0.03)	40.4(3.7)	90.4(1.5)	8	0.13	9.6
26.80	−0.34	0.45(0.02)	37.2(1.7)	100.3(0.7)	8	0.11	7.6
26.88	−0.30	0.40(0.03)	49.9(4.9)	101.4(1.7)	8	0.13	10.3
26.97	−0.25	0.61(0.03)	46.3(2.4)	90.3(1.0)	8	0.17	5.5
27.06	−0.20	0.68(0.03)	42.7(2.3)	92.8(1.0)	8	0.16	8.0
27.15	−0.16	0.38(0.02)	23.0(1.4)	88.4(0.6)	8	0.11	8.6
27.24	−0.11	0.60(0.02)	21.1(0.8)	95.0(0.4)	8	0.11	11.5
27.33	−0.06	0.53(0.02)	24.1(1.2)	94.5(0.5)	8	0.13	8.9
27.42	−0.02	0.52(0.03)	24.2(1.5)	90.8(0.6)	8	0.13	10.0
27.50	+0.03	0.59(0.05)	15.4(1.4)	94.5(0.6)	8	0.15	8.3
27.59	+0.07	0.61(0.04)	21.1(1.4)	94.5(0.6)	8	0.13	10.2
27.68	+0.12	0.50(0.03)*	16.3(1.2)	88.9(0.5)	8	0.13	8.5
27.77	+0.16	0.31(0.02)	33.0(2.9)	92.8(1.2)	8	0.10	10.1
27.86	+0.21	0.35(0.02)	39.8(3.1)	88.9(1.2)	8	0.17	6.8
27.95	+0.26	0.65(0.02)	29.8(1.1)	85.0(0.5)	8	0.10	8.2
28.04	+0.31	0.53(0.02)	34.8(1.9)	92.1(0.8)	5	0.14	15.0
28.13	+0.35	0.41(0.02)	31.1(1.4)	89.3(0.6)	8	0.08	18.6
28.21	+0.40	0.45(0.02)	48.7(2.9)	91.7(1.0)	8	0.14	7.6
28.30	+0.44	0.53(0.03)	24.2(1.8)	100.3(0.7)	8	0.14	9.2
Field 6a (G34.2+0.0) (see Fig. 10 for spectra)							
33.05	−0.02				8	0.13	12.4
33.14	+0.03				8	0.16	12.4
33.28	−0.02				8	0.14	11.1
33.37	+0.03				8	0.12	14.1
33.50	−0.02				8	0.13	15.2
33.59	+0.03				8	0.13	18.6
33.73	−0.02				8	0.13	10.8
33.82	+0.03				8	0.12	13.0
33.95	−0.02				8	0.16	10.6
34.04	+0.03				8	0.15	9.4
34.18	−0.02				5	0.18	9.7
34.27	+0.03	0.38(0.03)	16.8(1.4)	47.4(0.6)	8	0.10	13.1
34.40	−0.02				8	0.19	9.0
34.49	+0.03				8	0.14	12.2
34.63	−0.02				8	0.14	9.8
34.72	+0.03				8	0.10	13.3
34.85	−0.02				8	0.14	8.9
34.94	+0.03	0.35(0.02)	39.0(2.5)	56.5(1.0)	8	0.12	11.0
35.08	−0.02	0.30(0.02)	38.6(3.0)	52.4(1.2)	8	0.10	8.9
35.17	+0.03				8	0.20	11.9

Table 1. *(Continued).*

l (^{o})	b (^{o})	T_L/T_{sys} $\times 10^3$	ΔV (km s^{-1})	$V_{\rm LSR}$ (km s^{-1})	V_{res} (km s^{-1})	RMS[1] $\times 10^3$	t_{int} (hrs)
Field 6b (G36.5+0.0) (see Fig. 11 for spectra)							
35.31	−0.02	0.32(0.02)	45.4(3.4)	54.2(1.4)	8	0.11	11.1
35.40	+0.03	0.36(0.02)	45.1(2.3)	57.5(1.0)	8	0.10	14.3
35.53	−0.02	0.56(0.02)	36.7(1.6)	55.9(0.7)	8	0.16	7.2
35.62	+0.03				8	0.13	9.4
35.76	−0.02	0.21(0.02)*	31.6(3.8)	60.5(1.5)	6	0.10	10.7
35.85	+0.02				8	0.13	13.0
35.98	−0.02				8	0.13	11.7
36.07	+0.03				5	0.13	13.0
36.21	−0.02				8	0.12	10.6
36.30	+0.02				8	0.16	13.8
36.43	−0.02	0.61(0.03)	21.2(1.5)	82.0(0.6)	8	0.13	10.9
		0.46(0.03)	25.3(2.3)	47.5(0.89)	8	0.13	10.9
36.52	+0.02	0.27(0.02)	47.1(3.8)	71.9(1.5)	8	0.11	9.0
36.66	−0.02	0.43(0.03)	26.1(2.1)	79.3(0.9)	8	0.11	10.8
36.75	+0.02				8	0.12	13.0
36.89	−0.02				8	0.15	9.9
37.11	−0.02				8	0.17	12.2
37.20	+0.03	0.29(0.02)	46.2(3.4)	69.8(1.3)	8	0.11	14.2
37.34	−0.02	0.48(0.03)	31.5(2.2)	73.8(0.9)	8	0.17	5.4
37.43	+0.02				8	0.15	9.9
Field 6c (G38.7+0.0) (see Fig. 12 for spectra)							
37.56	−0.02				8	0.14	12.0
37.65	+0.02				8	0.15	15.5
37.79	−0.02				8	0.15	14.4
37.88	+0.02				8	0.17	8.4
38.01	−0.02	0.46(0.03)	46.7(3.3)	59.8(1.4)	8	0.14	9.3
38.10	+0.02				8	0.14	14.0
38.24	−0.03	0.33(0.02)	51.6(3.5)	58.6(1.4)	8	0.12	8.6
38.33	+0.02				8	0.16	9.1
38.46	−0.03	0.50(0.03)	21.5(1.6)	40.0(0.7)	8	0.13	9.7
38.55	+0.02				8	0.13	12.5
38.69	−0.03				8	0.19	6.8
38.78	+0.02				8	0.14	9.1
38.91	−0.03				8	0.15	10.9
39.00	+0.02				8	0.11	12.3
39.14	−0.02				8	0.26	2.6
39.22	+0.03				8	0.21	4.9
39.36	−0.02				8	0.20	4.3
39.45	+0.03				8	0.19	5.9
39.59	−0.02				8	0.18	4.2
39.68	+0.03				8	0.16	6.6

Table 1. (*Continued*).

l (^{o})	b (^{o})	T_L/T_{sys} $\times 10^3$	ΔV (km s^{-1})	$V_{\rm LSR}$ (km s^{-1})	V_{res} (km s^{-1})	RMS[1] $\times 10^3$	t_{int} (hrs)
Field 7 (G45.5+0.0) (see Fig. 13 for spectra)							
44.67	−0.44	0.30(0.03)*	28.3(2.9)	56.1(1.2)	8	0.12	9.0
44.76	−0.40				8	0.14	9.5
44.85	−0.35				8	0.12	10.4
44.94	−0.30				8	0.12	9.2
45.03	−0.25				8	0.13	10.5
45.12	−0.21				8	0.10	13.8
45.20	−0.16				8	0.10	10.3
45.29	−0.11				8	0.11	12.0
45.38	−0.07				8	0.10	10.5
45.47	−0.02	0.42(0.02)*	11.2(0.7)	55.1(0.3)	8	0.10	14.6
45.56	+0.03	0.38(0.02)	36.2(2.4)	44.9(1.0)	8	0.13	9.8
45.64	+0.08				8	0.12	15.1
45.73	+0.12				8	0.19	6.3
45.82	+0.17				8	0.14	11.0
45.91	+0.22				8	0.13	10.2
46.00	+0.26				8	0.16	10.3
46.08	+0.31				8	0.14	9.6
46.17	+0.36				8	0.11	9.7
46.26	+0.41	0.53(0.04)	16.0(1.3)	43.9(0.5)	8	0.10	9.5
		0.28(0.04)	17.0(2.5)	12.8(1.0)	8	0.10	9.5
46.35	+0.45				8	0.12	11.7
Field 8 (G56.9+0.0) (see Fig. 14 for spectra)							
56.08	−0.46	0.47(0.03)	32.7(2.7)	23.0(1.1)	8	0.13	12.8
56.17	−0.42	0.24(0.02)	30.6(3.5)	24.5(1.4)	8	0.10	13.7
56.26	−0.37	0.35(0.03)	54.8(6.8)	37.0(2.5)	8	0.15	9.9
56.34	−0.32				8	0.14	12.7
56.43	−0.27	0.33(0.03)*	25.2(2.8)	31.3(1.1)	8	0.13	12.5
56.52	−0.22				8	0.09	16.1
56.60	−0.17	0.37(0.02)	37.3(3.4)	24.3(1.2)	8	0.13	8.2
56.69	−0.12				8	0.13	12.4
56.78	−0.07	0.47(0.03)	27.6(2.4)	23.8(1.0)	8	0.14	10.1
56.86	−0.02				8	0.15	13.2
56.95	+0.03	0.21(0.01)*	32.4(2.5)	25.3(1.0)	8	0.08	13.1
57.04	+0.08	0.21(0.02)	49.5(7.0)	13.5(2.4)	8	0.10	16.8
57.12	+0.13	0.22(0.02)	64.3(11.2)	15.0(3.1)	8	0.11	11.1
57.21	+0.18				8	0.16	15.1
57.30	+0.23	0.39(0.02)	29.0(1.7)	12.5(0.6)	8	0.12	8.6
57.38	+0.28				8	0.10	11.6
57.47	+0.33				8	0.16	9.5
57.56	+0.38	0.27(0.02)	44.4(3.1)	17.2(1.3)	8	0.12	12.0
57.65	+0.42	0.30(0.02)	51.7(3.7)	19.7(1.4)	8	0.13	9.5
57.73	+0.47				8	0.15	11.4

Table 1. *(Continued).*

l (^{o})	b (^{o})	T_L/T_{sys} $\times 10^3$	ΔV (km s^{-1})	$V_{\rm LSR}$ (km s^{-1})	V_{res} (km s^{-1})	RMS[1] $\times 10^3$	t_{int} (hrs)
Field 9 (G66.2+0.0) (see Fig. 15 for spectra)							
65.39	−0.50	0.38(0.02)	44.7(2.8)	13.0(1.2)	8	0.10	11.6
65.48	−0.45	0.44(0.03)	37.5(3.1)	5.4(1.3)	8	0.13	12.1
65.56	−0.39	0.33(0.03)	44.7(4.4)	4.8(1.5)	8	0.13	8.9
65.65	−0.34				8	0.12	9.6
65.73	−0.29				8	0.15	5.8
65.82	−0.24				8	0.14	10.8
65.90	−0.18				8	0.13	12.1
65.99	−0.13				8	0.08	17.3
66.08	−0.08				8	0.16	4.8
66.16	−0.03				8	0.16	4.1
66.24	+0.03	0.67(0.02)	43.9(1.6)	14.9(0.7)	8	0.14	8.8
66.33	+0.08	0.42(0.04)	44.3(4.5)	3.2(1.8)	8	0.15	11.1
66.41	+0.13				8	0.22	7.5
66.50	+0.19				8	0.19	8.4
66.59	+0.24				8	0.13	11.5
66.67	+0.29				8	0.11	13.8
66.75	+0.35	0.33(0.03)*	38.2(4.2)	10.2(1.8)	8	0.15	7.7
66.84	+0.40	0.27(0.02)*	42.6(3.4)	8.3(1.4)	8	0.11	12.2
66.92	+0.45				8	0.16	8.5
67.01	+0.50				8	0.14	9.4

[1] RMS is in units of T_L/T_{sys}.

* Tentative detection.

Table 2. Line parameters from the low resolution observation and the average spectrum.

Field Name	l ($b = 0^o$) (^{o})	T_L/T_{sys} $\times 10^3$	ΔV (km s^{-1})	$V_{\rm LSR}$ (km s^{-1})	V_{res} (km s^{-1})	RMS[1] $\times 10^3$	t_{int} (hrs)
Field 1	348.0#	0.51(0.02)	35.9(1.5)	−15.5(0.6)	2	0.08	214.1
	348.0!	0.42(0.02)	53.6(2.9)	−22.6(1.2)	8	0.12	12.7
Field 2b	2.3#	0.43(0.01)	29.2(1.1)	5.1(0.5)	2	0.06	207.9
	2.3!	0.37(0.02)	26.0(2.0)	10.2(0.8)	8	0.10	10.7
Field 2c	4.7#	0.56(0.01)	34.3(1.0)	8.6(0.4)	2	0.06	199.5
	4.7!	0.67(0.02)	28.7(0.9)	11.3(0.4)	8	0.09	13.2
Field 3	13.9#	0.76(0.02)	34.9(0.8)	27.5(0.3)	2	0.07	182.9
	13.9!	0.90(0.02)	37.7(0.7)	26.7(0.3)	8	0.08	16.8
Field 4	25.2#	0.28(0.01)	30.0(1.7)	101.8(0.7)	3	0.06	205.8
	25.2!	0.44(0.01)	25.5(0.8)	98.2(0.4)	6	0.10	19.8
Field 5	27.5#	0.43(0.01)	31.9(1.0)	92.7(0.4)	3	0.05	189.7
	27.5!	0.39(0.02)	28.5(1.4)	91.6(0.6)	8	0.08	18.2
Field 6a	34.2#	0.15(0.02)	15.2(1.8)	90.4(0.8)	3	0.05	235.2
		0.17(0.01)	27.9(2.2)	50.8(0.9)	3	0.05	235.2
	34.2!	0.26(0.02)	14.2(0.9)	45.6(0.4)	5	0.08	38.4
Field 6b	36.5#	0.27(0.01)	55.6(2.4)	64.7(1.0)	5	0.06	209.1
	36.5!	0.25(0.01)	60.0(3.2)	65.2(1.2)	8	0.07	33.5
Field 6c	38.7#				3	0.09	181.1
	38.7!				8	0.07	27.6
Field 7	45.5#	0.18(0.01)	44.6(2.6)	47.5(1.1)	3	0.05	213.0
	45.5!	0.20(0.01)	40.5(2.2)	48.8(0.9)	8	0.05	53.5
Field 8	56.9#	0.24(0.01)	48.0(2.1)	21.2(0.9)	5	0.05	240.3
	56.9!	0.25(0.01)	21.2(1.6)	20.9(0.7)	8	0.06	46.2
Field 9	66.2#	0.25(0.01)	49.1(1.7)	9.9(0.7)	5	0.04	196.0
	66.2!				8	0.07	45.2

[1] RMS is in units of T_L/T_{sys}.

Parameters from the average spectrum.

! Parameters from the spectrum obtained with a 2° × 2° beam (paper I).

Table 3. H II regions and RRLs near 327 MHz in field 7 (G45.5+0.0).

l (^{o})	b (^{o})	T_L (mK).	ΔV (km s^{-1})	$V_{\rm LSR}$ (km s^{-1})	λ_{obs} (cm)	Note
44.786	−0.490	17(2.5)	30.0(5.5)	44.8(4.0)	9	L89
44.981	−0.646	14(2.0)	20.3(3.4)	67.3(1.4)	9	lph96
45.125	0.136	67(4.9)	31.6(2.7)	57.6(1.1)	3	L89
45.451	0.060	153(6.3)	27.9(1.3)	55.9(0.6)	3	L89
45.475	0.130	57(3.9)	27.5(2.1)	56.0(0.9)	3	L89
45.824	−0.290	16(2.0)	38.7(5.8)	62.3(4.2)	3	L89
46.495	−0.247	83(5.1)	22.4(1.6)	57.2(0.7)	3	L89
RRLs near 327 MHz in field 7						
l (^{o})	b (^{o})	T_L/T_{sys}	ΔV (km s^{-1})	$V_{\rm LSR}$ (km s^{-1})		Note
44.67	−0.44	0.30(0.03)	28.3(2.9)	56.1(1.2)		t
45.47	−0.02	0.42(0.02)	11.2(0.7)	55.1(0.3)		t
45.56	+0.03	0.38(0.02)	36.2(2.4)	44.9(1.0)		
46.26	+0.41	0.53(0.04)	16.0(1.3)	43.9(0.5)		
		0.28(0.04)	17.0(2.5)	12.8(1.0)		

Note: L89 – Lockman (1989); lph96 – Lockman *et al.*(1996);
t – Tentative detection.

Table 4. Line parameters from the set of average spectra in field 7 (G45.5+0.0).

l (°)	b (°)	T_L/T_{sys} $\times 10^3$	ΔV (km s^{-1})	$V_{\rm LSR}$ (km s^{-1})	V_{res} (km s^{-1})	RMS[1] $\times 10^3$	t_{int} (hrs)
Average over 2° × 12′							
46.30	+0.43	0.33(0.02)	33.0(1.1)	53.4(0.5)	8	0.09	21.1
46.12	+0.34				8	0.09	19.3
45.95	+0.24				8	0.10	20.5
45.77	+0.14	0.34(0.03)	13.6(1.3)	57.6(0.6)	5	0.13	17.3
45.60	+0.05	0.28(0.01)	39.8(2.5)	47.6(1.0)	8	0.08	24.8
45.43	−0.04	0.33(0.03)	11.7(1.1)	55.0(0.5)	3	0.12	25.2
45.25	−0.13	0.24(0.04)*	10.1(2.1)	53.2(0.9)	3	0.11	22.3
45.07	−0.23	0.18(0.02)*	26.4(3.8)	55.5(1.5)	5	0.09	24.3
		0.23(0.02)*	19.4(2.6)	18.4(1.0)	5	0.09	24.3
44.89	−0.33	0.29(0.03)*	11.6(1.2)	56.9(0.5)	3	0.11	19.5
44.71	−0.42	0.37(0.04)	10.4(1.4)	56.0(0.6)	3	0.12	18.5
Average over 2° × 30′							
46.17	+0.36	0.15(0.02)	9.1(1.2)	62.9(0.5)	8	0.06	50.7
		0.21(0.01)	15.8(1.2)	41.9(0.5)	8	0.06	50.7
45.73	+0.12	0.30(0.02)	14.2(1.0)	59.0(0.4)	6	0.07	52.4
		0.17(0.01)	29.3(3.2)	33.4(1.2)	6	0.07	52.4
45.29	−0.11	0.20(0.02)*	17.4(1.9)	54.9(0.8)	5	0.07	61.3
44.85	−0.35	0.30(0.03)	11.7(1.3)	56.0(0.5)	3	0.08	48.6
Average over 2° × 1°							
45.95	+0.24	0.14(0.01)	35.2(2.6)	47.5(1.1)	6	0.05	103.1
45.07	−0.23	0.24(0.02)	12.8(1.1)	55.3(0.5)	5	0.05	109.9

[1] RMS is in units of T_L/T_{sys}

* Tentative detection.

APPENDIX 2

This Appendix, beginning on the next page, contains all the figures (Fig. 1 to Fig. 19) referred to in this paper.

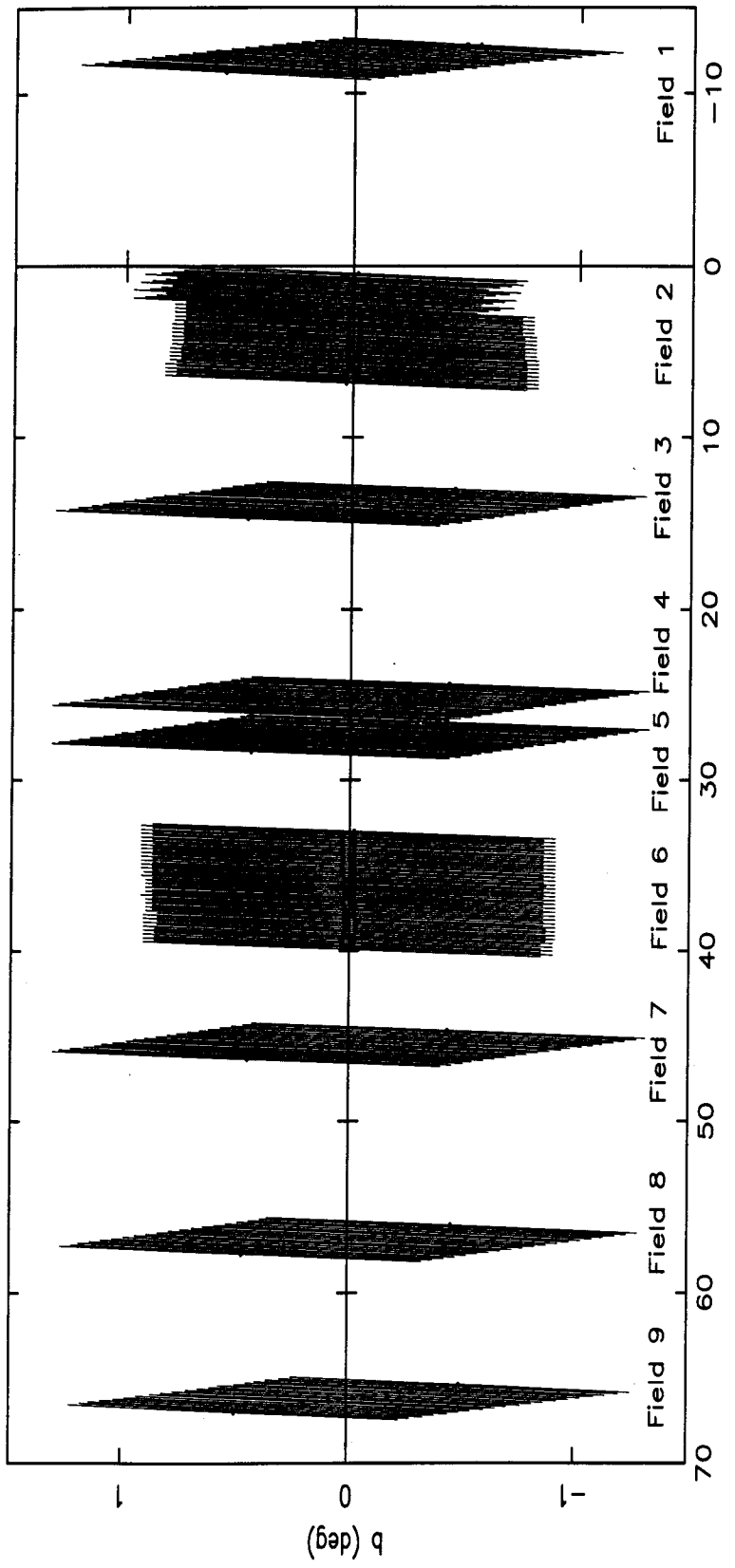

Figure 1. The positions observed in the galactic plane with the 2° × 6′ beam of the ORT are shown schematically in galactic coordinates. The dots indicate the beam center and the length of the line represent the extent of the 2° beam of the ORT. Except for fields 2 and 6, the beam centers were chosen so that a set of 20 adjacent positions in declination correspond to a 2° × 2° region from which RRLs were observed in the low-resolution survey (paper I). For fields 2 and 6, the center of the two beams, from which RRLs were observed simultaneously in this survey, is positioned along the galactic plane. Since the ORT is a north-south oriented telescope the 2° × 2° beam is inclined with respect to the galactic plane.

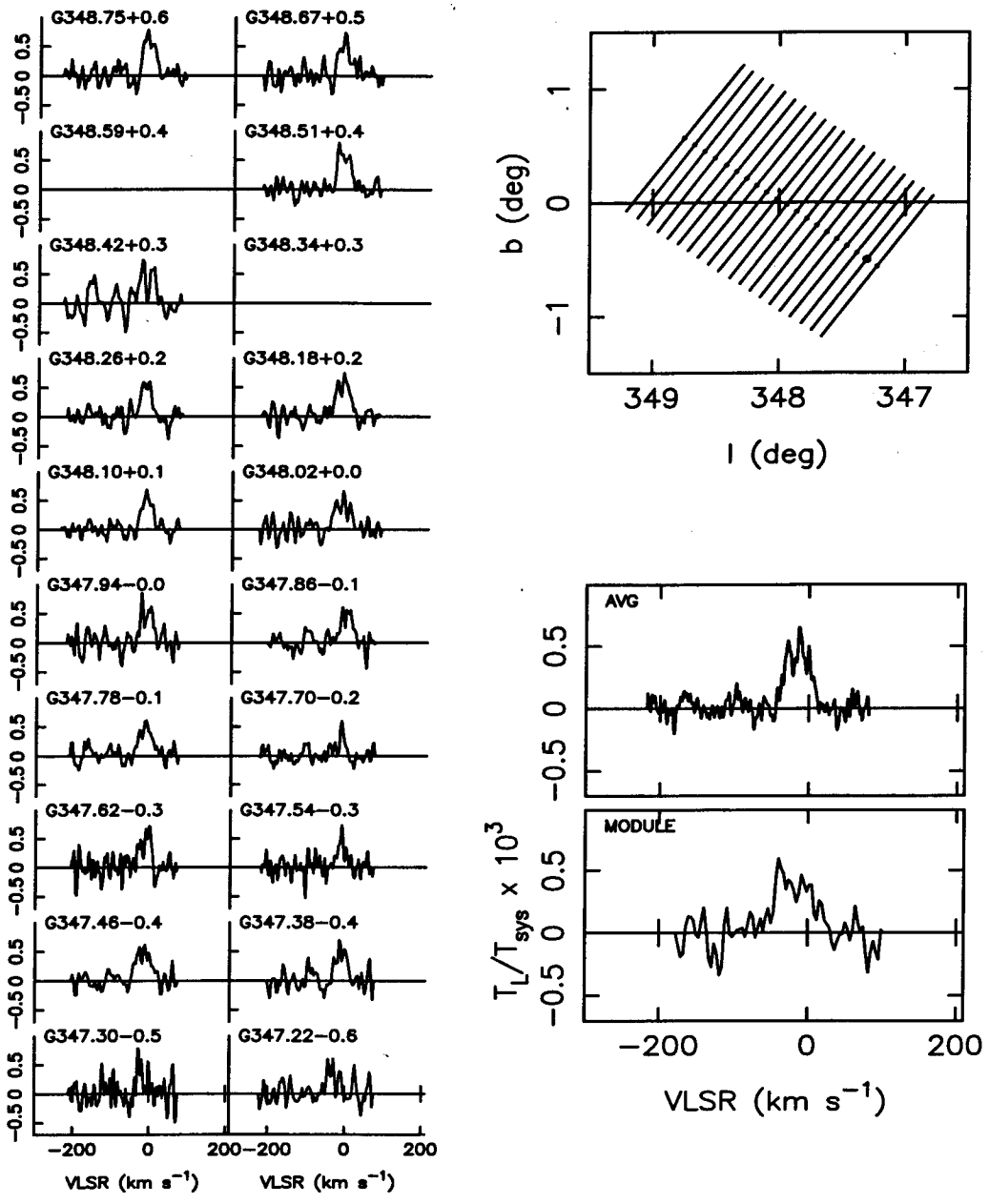

Figure 2. Spectra of recombination lines near 327 MHz observed with a beam of 2° × 6′ towards various positions within field 1 centered at G348.0+0.0 are shown on the left. The positions observed are shown schematically in galactic coordinates in the top right corner where the dots indicate the beam center and the length of the line represent the extent of the 2° beam of the ORT. The spectrum (labeled as AVG) obtained by averaging all the 20 spectra and the spectrum (labeled as MODULE) obtained using a 2° × 2° beam covering the same region (taken from paper I) are shown in the bottom right corner. The ordinate of the spectra are in units of T_L/T_{sys} and abscissa are in LSR velocity with respect to the hydrogen line.

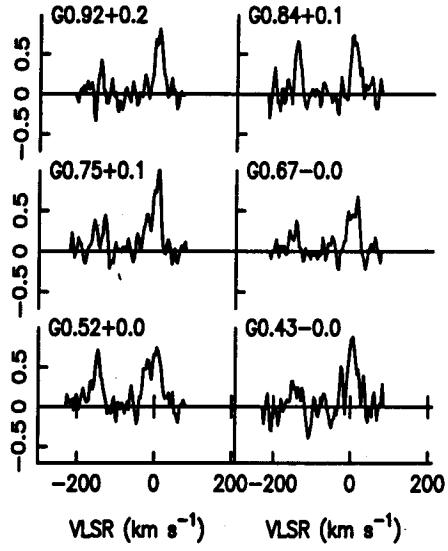

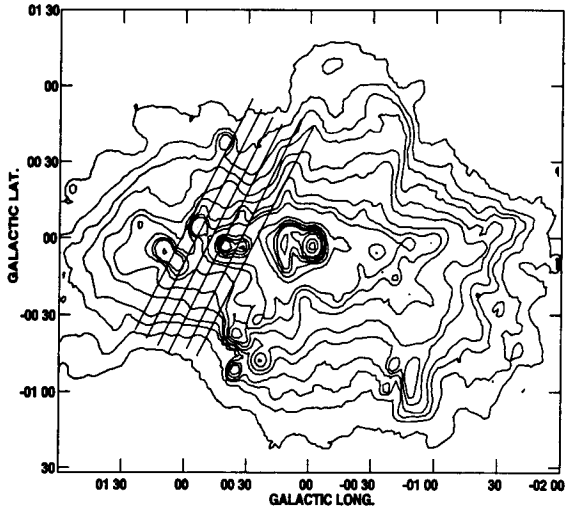

Figure 3. Spectra of recombination lines near 327 MHz observed with a beam of 2° × 6′ towards various positions within field 2a are shown on top. The observed positions are shown by slanted lines marked on the 11 cm continuum map with an angular resolution of 4′.3 taken from Reich *et al.* (1990) (bottom). The slanted line represent the 2° × 6′ beam of the ORT. The ordinate of the spectra are in units of T_L/T_{sys} and abscissa are in LSR velocity with respect to the hydrogen line. The contour levels for the 11 cm continuum map are in brightness temperatures of 0.5, 1, 1.5, 2, 3, 4, 5, 6, 8, 10, 20, 30, 40, 50, 70, 100, 200, 300 K.

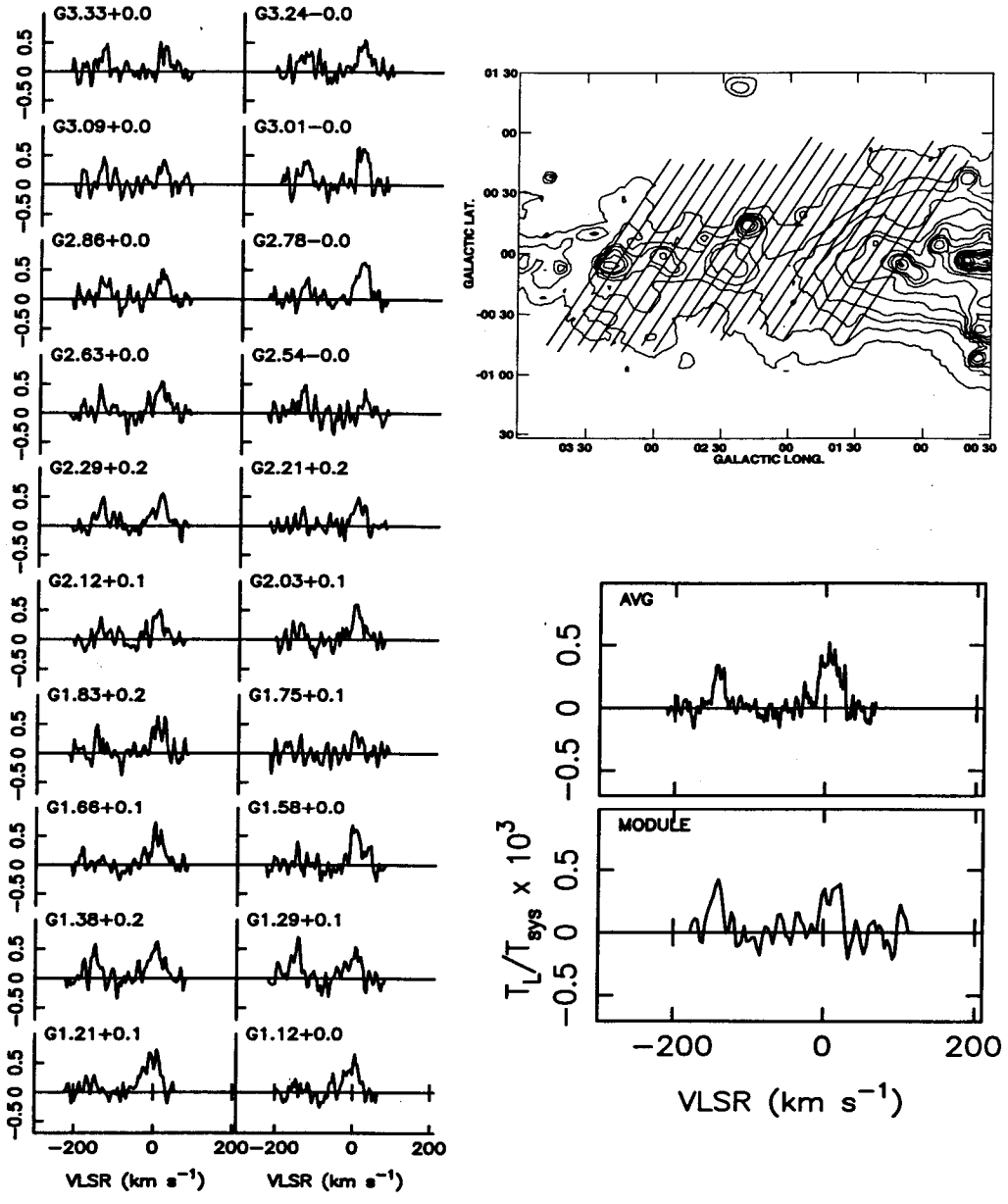

Figure 4. Spectra of recombination lines near 327 MHz observed with a beam of 2° × 6′ towards various positions within field 2b centered at G2.3+0.0 are shown on the left. The observed positions are shown by slanted lines marked on the 11 cm continuum map with an angular resolution of 4′.3 taken from Reich *et al.* (1990) (top right corner). The slanted line represent the 2° × 6′ beam of the ORT. The spectrum (labeled as AVG) obtained by averaging all the 20 spectra and the spectrum (labeled as MODULE) obtained using a 2° × 2° beam covering the same region (taken from paper I) are shown in the bottom right corner. The ordinate of the spectra are in units of T_L/T_{sys} and abscissa are in LSR velocity with respect to the hydrogen line. The contour levels for the 11 cm continuum map are in brightness temperatures of 0.5, 1, 1.5, 2, 3, 4, 6, 8, 10, 15, 20, 25, 30, 40, 50, 60 K.

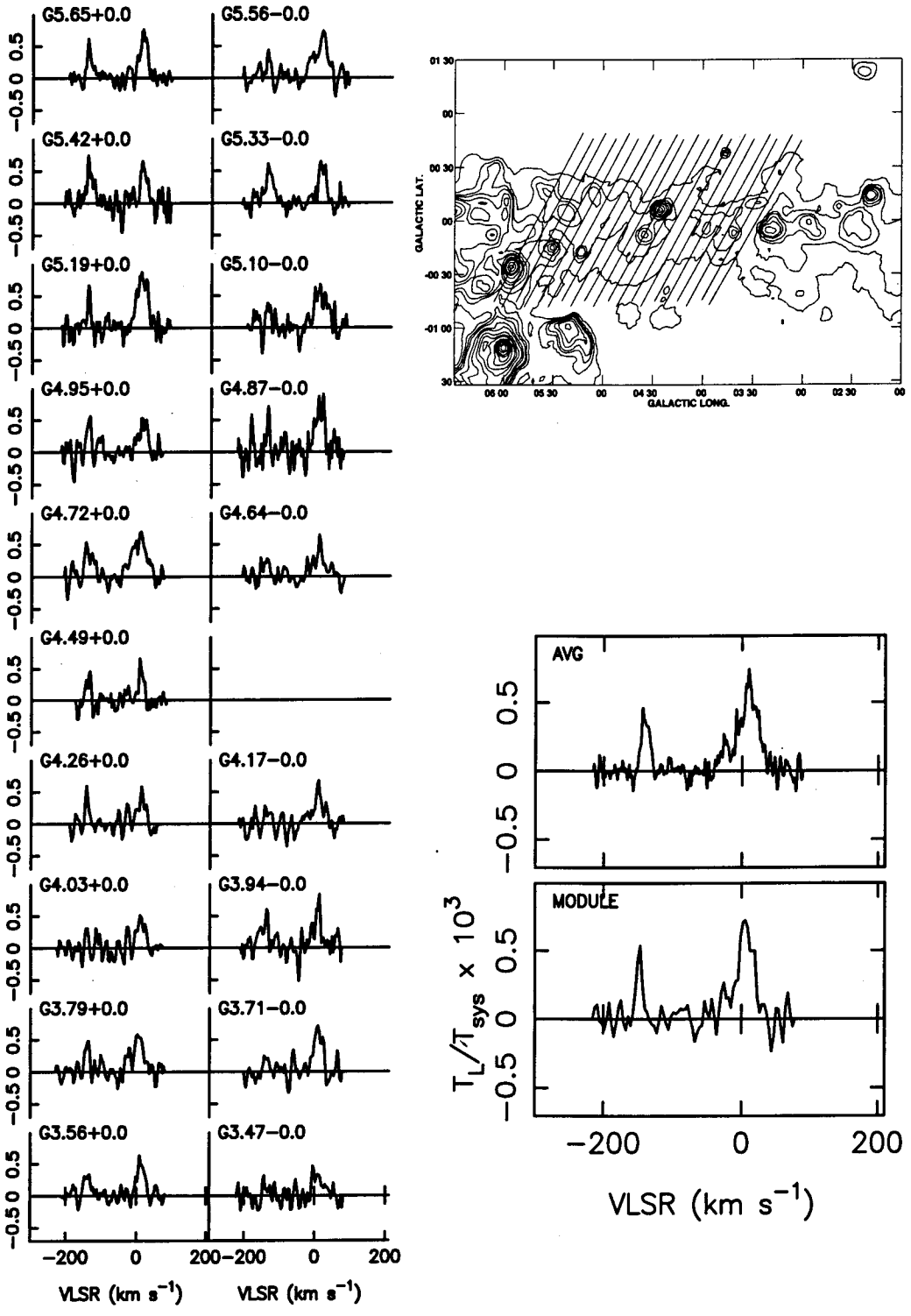

Figure 5. Same as Fig 4 for the field 2c centered at G4.7+0.0. The contour levels for the 11 cm continuum map are in brightness temperatures of 0.5, 1, 1.5, 2, 3, 4, 6, 8, 10, 15, 20, 25, 30, 40, 50 K.

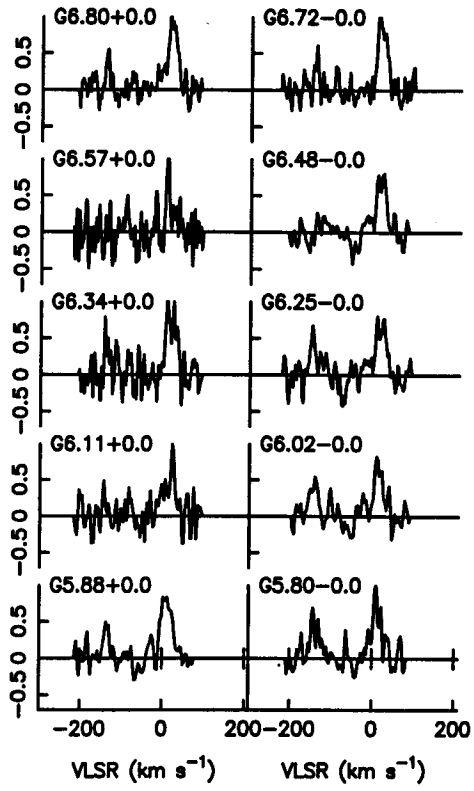

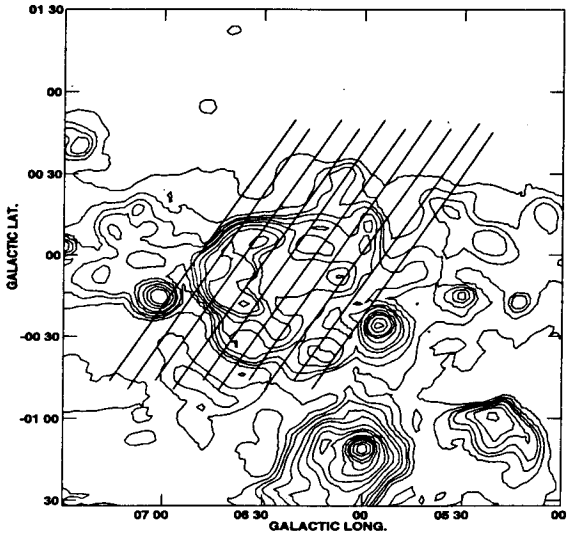

Figure 6. Same as Fig 3 for the field 2d. The contour levels for the 11 cm continuum map are in brightness temperatures of 0.5, 1, 1.5, 2, 3, 4, 6, 8, 10, 15, 20, 25, 30, 40, 50 K.

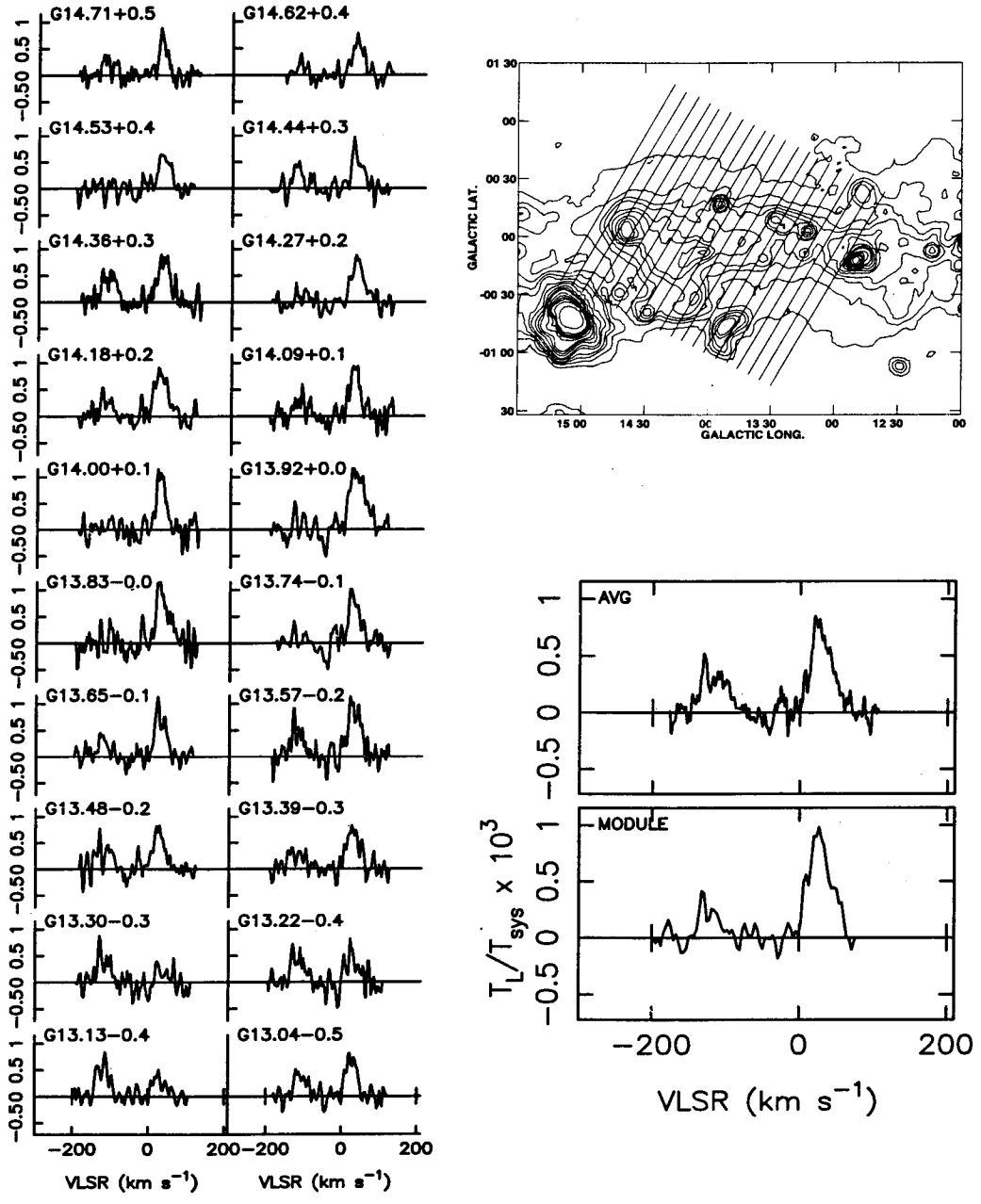

Figure 7. Same as Fig 4 for the field 3 centered at G13.9+0.0. The contour levels for the 11 cm continuum map are in brightness temperatures of 0.5, 1, 1.5, 2, 3, 4, 6, 8, 10, 15, 20, 25, 30, 40, 100 K.

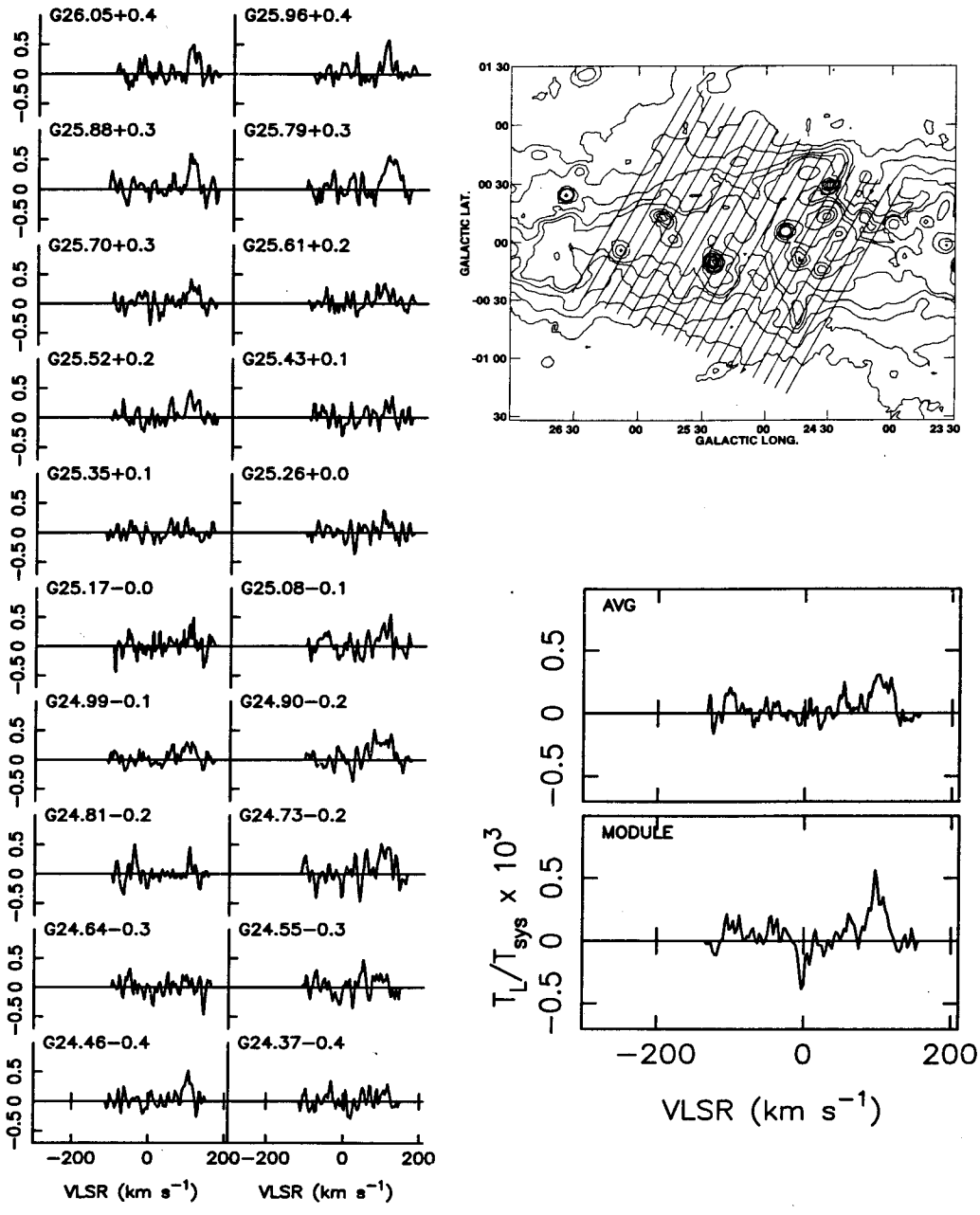

Figure 8. Same as Fig 4 for the field 4 centered at G25.2+0.0. The contour levels for the 11 cm continuum map are in brightness temperatures of 0.2, 0.5, 1, 1.5, 2, 4, 6, 8, 10, 15, 20, 25, 30 K.

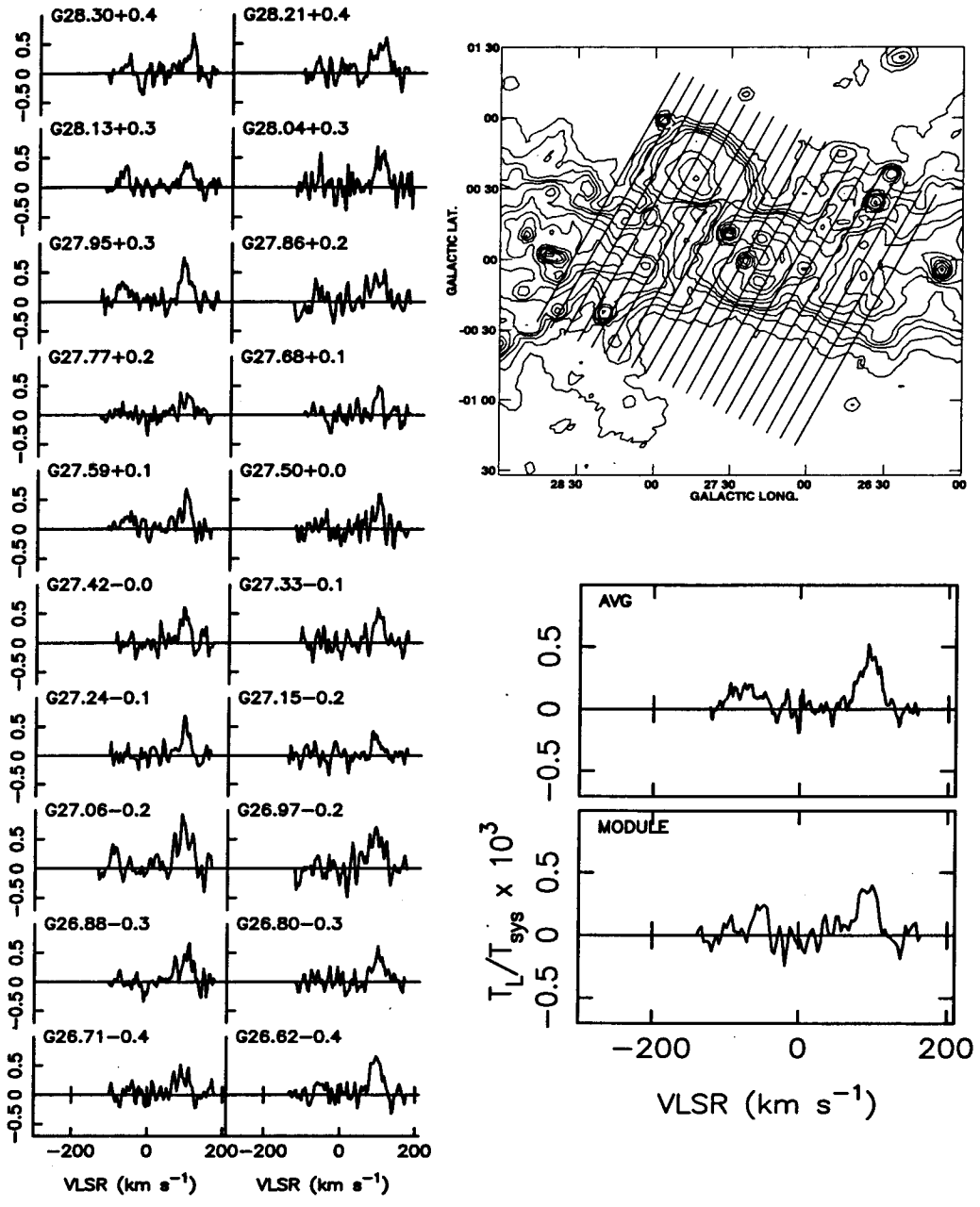

Figure 9. Same as Fig 4 for the field 5 centered at G27.5+0.0. The contour levels for the 11 cm continuum map are in brightness temperatures of 0.2, 0.4, 0.6, 0.8, 1, 1.5, 2, 3, 4, 5, 6, 7, 8 K.

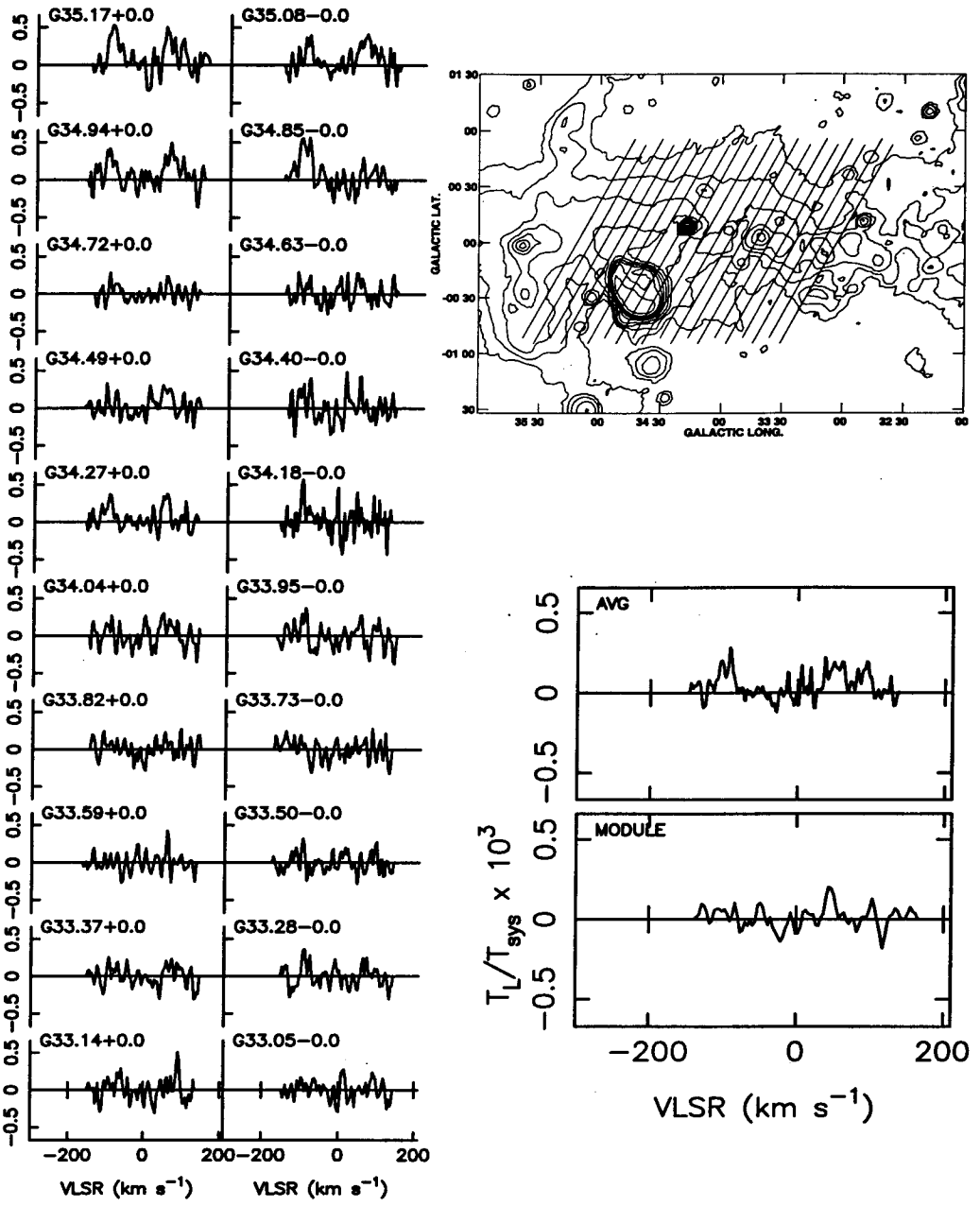

Figure 10. Same as Fig 4 for the field 6a centered at G34.2+0.0. The contour levels for the 11 cm continuum map are in brightness temperatures of 0.2, 0.5, 1, 2, 4, 6, 8, 10, 14, 18, 22, 24, 26 K.

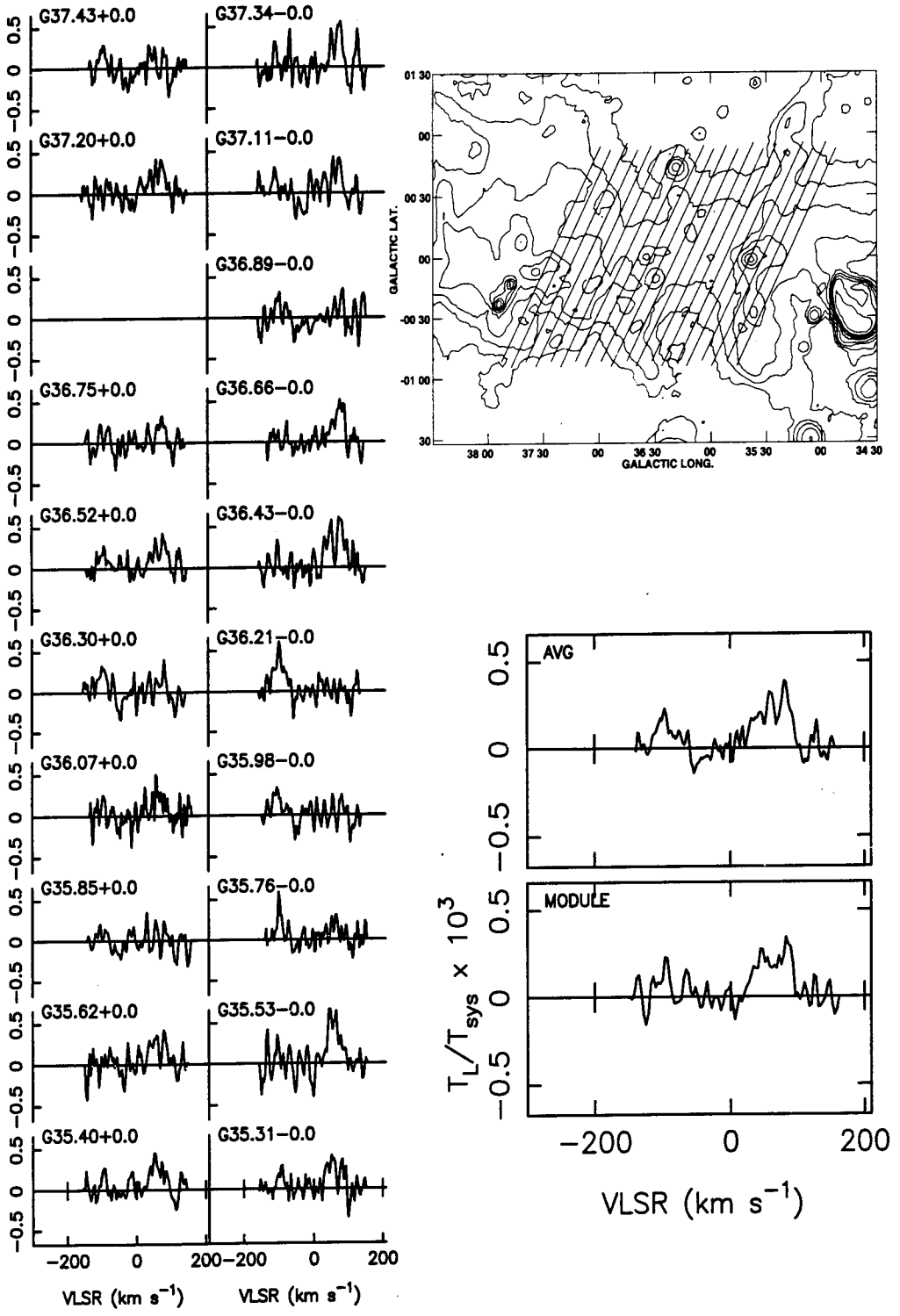

Figure 11. Same as Fig 4 for the field 6b centered at G36.5+0.0. The contour levels for the 11 cm continuum map are in brightness temperatures of 0.2, 0.5, 1, 2, 4, 6, 8, 10, 14, 18 K.

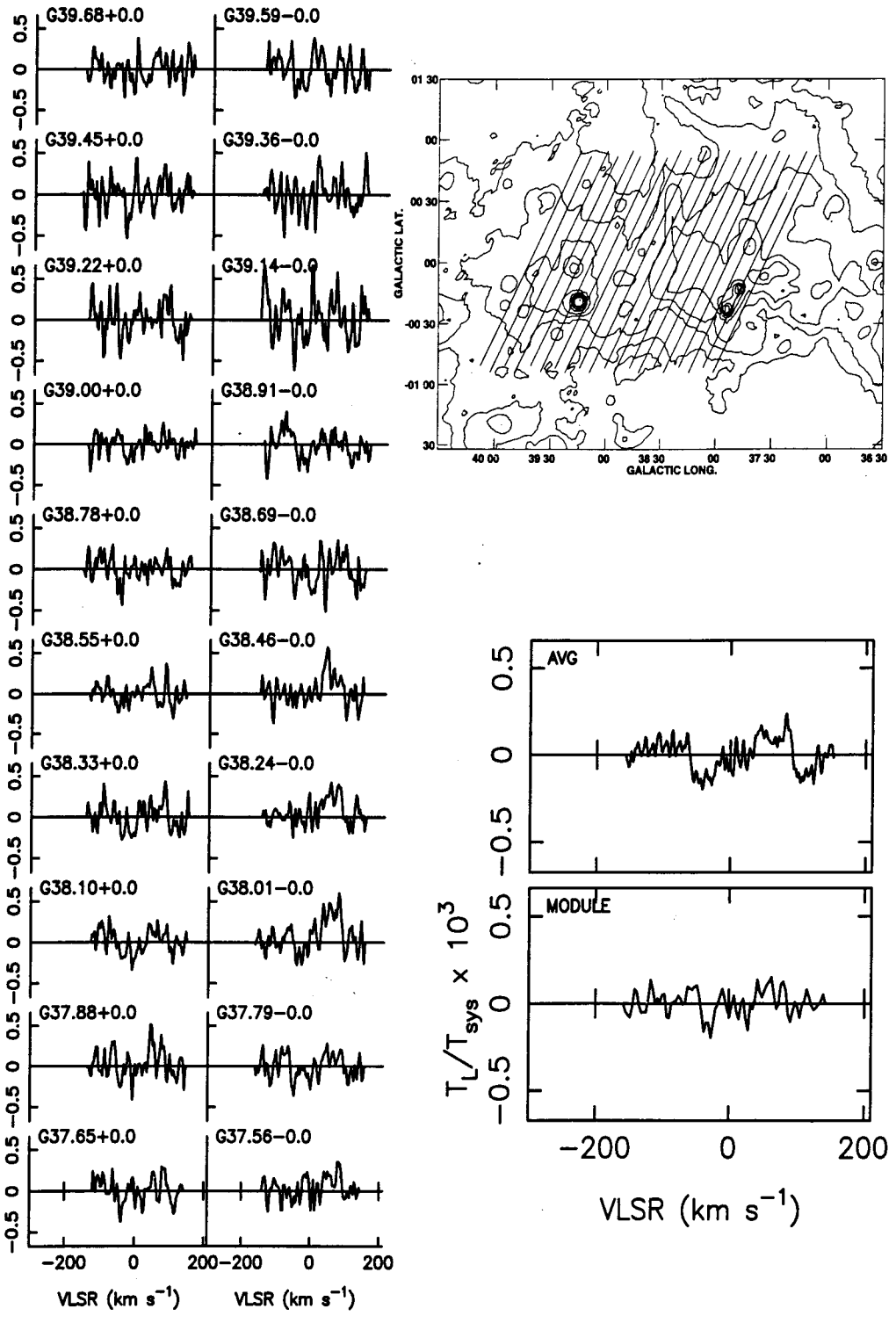

Figure 12. Same as Fig 4 for the field 6c centered at G38.7+0.0. The contour levels for the 11 cm continuum map are in brightness temperatures of 0.2, 0.5, 1, 2, 4, 6, 8, 10, 14, 18 K.

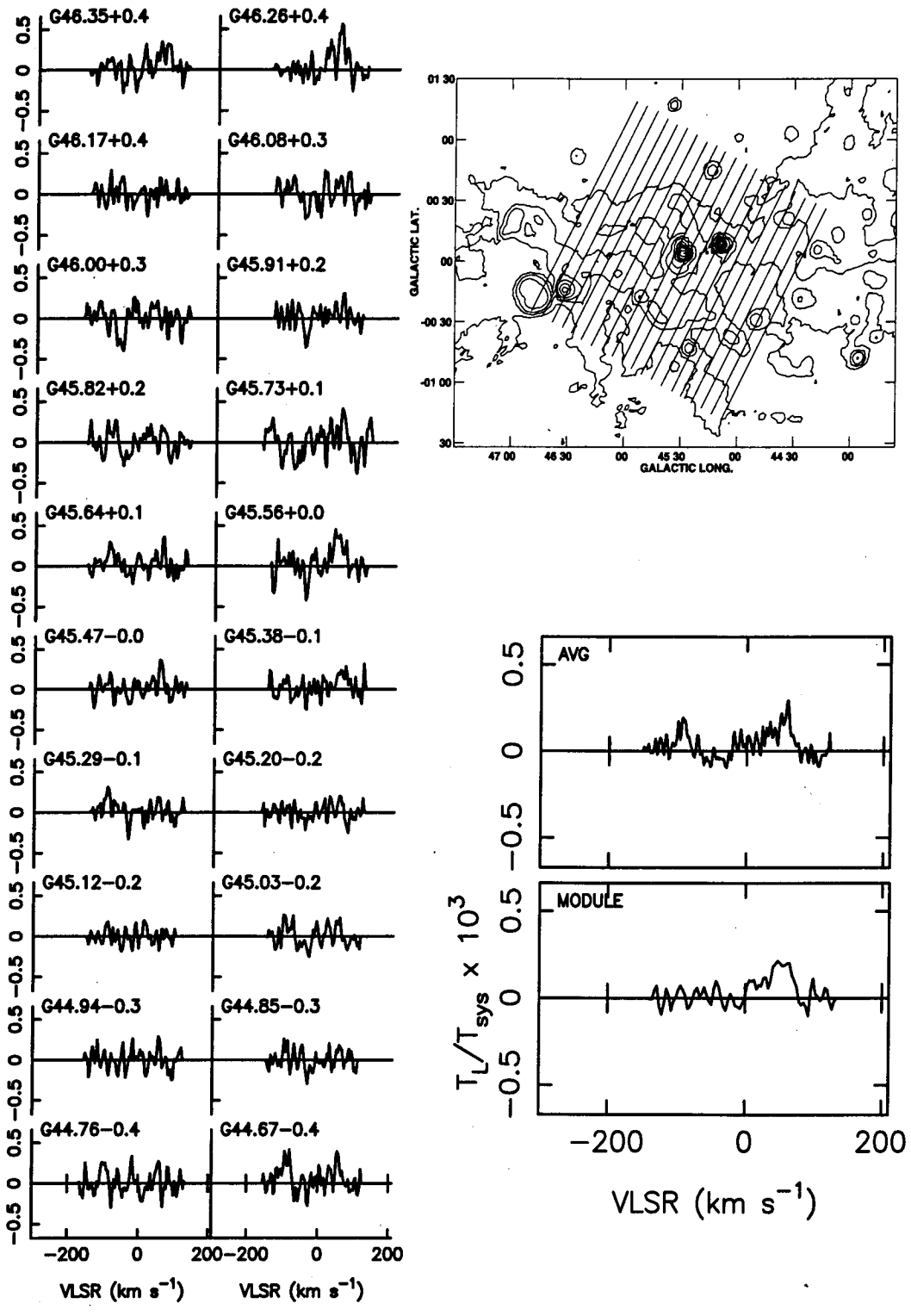

Figure 13. Same as Fig 4 for the field 7 centered at G45.5+0.0. The contour levels for the 11 cm continuum map are in brightness temperatures of 0.2, 0.5, 1, 2, 4, 6, 8, 10, 14, 18 K.

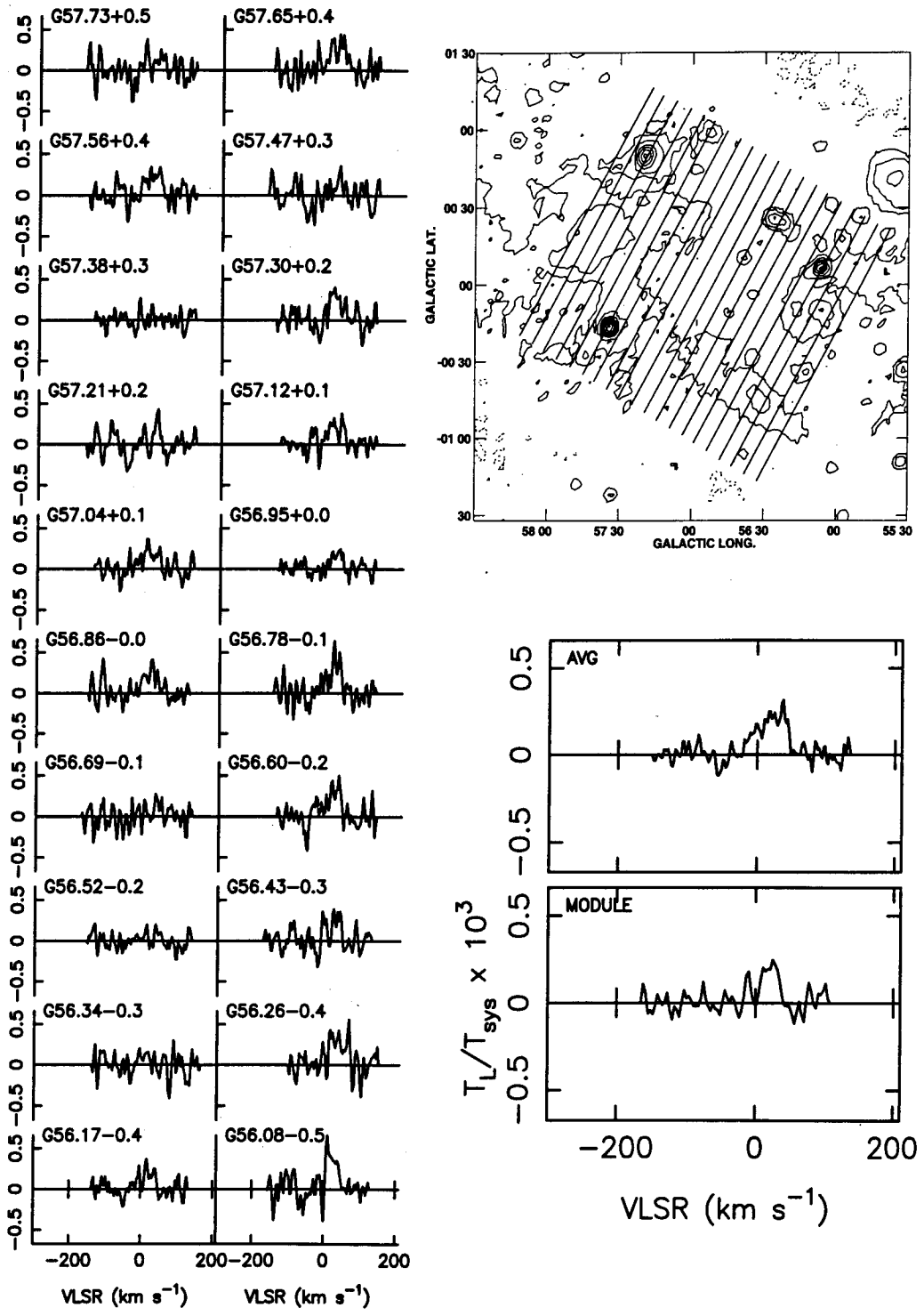

Figure 14. Same as Fig 4 for the field 8 centered at G56.9+0.0. The contour levels for the 11 cm continuum map are in brightness temperatures of −0.02, 0.1, 0.2, 0.4, 0.6, 0.8, 1, 1.2, 1.5, 1.9 K.

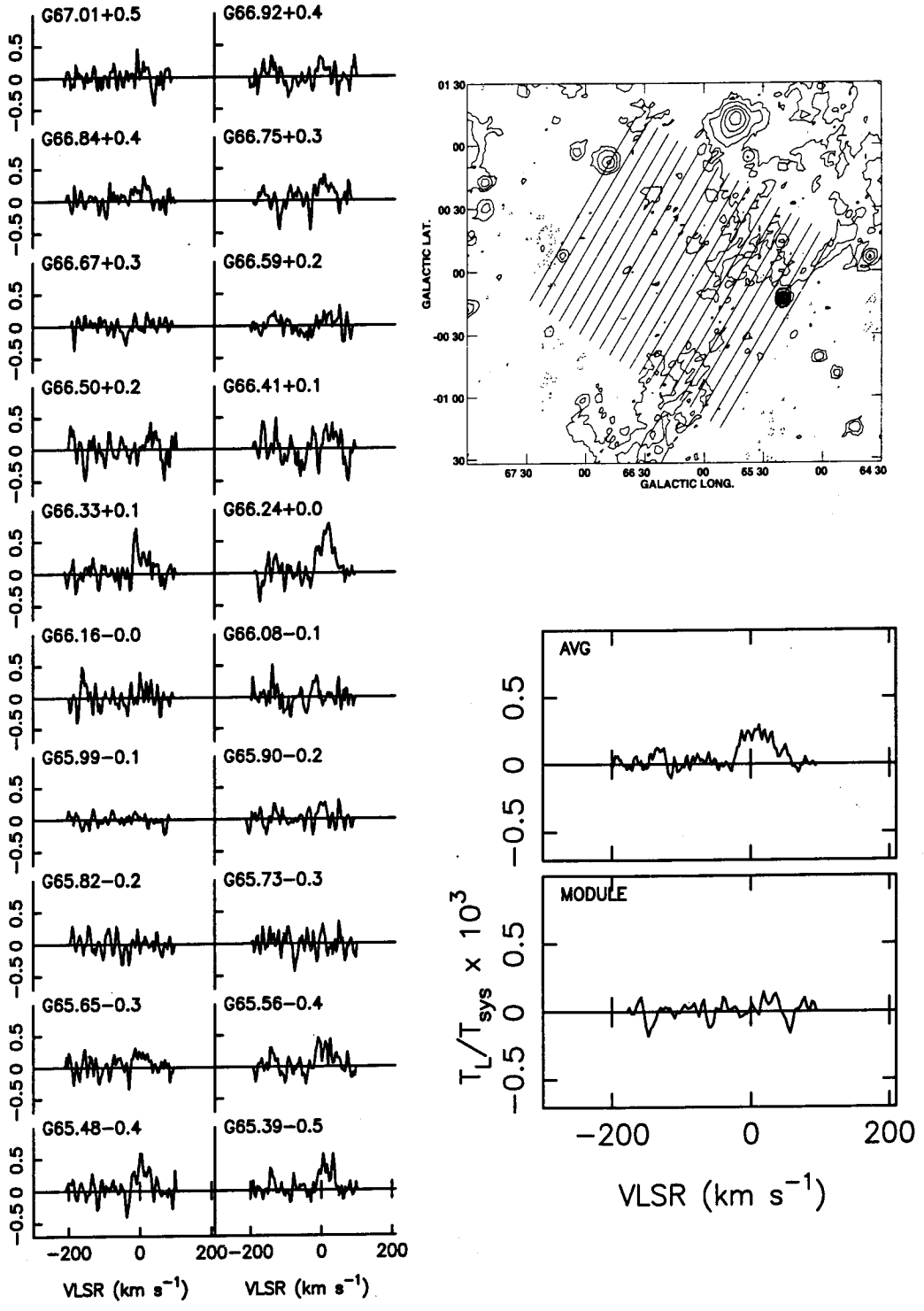

Figure 15. Same as Fig 4 for the field 9 centered at G66.2+0.0. The contour levels for the 11 cm continuum map are in brightness temperatures of −0.02, 0.1, 0.2, 0.4, 0.6, 0.8, 1, 1.2, 1.4 K.

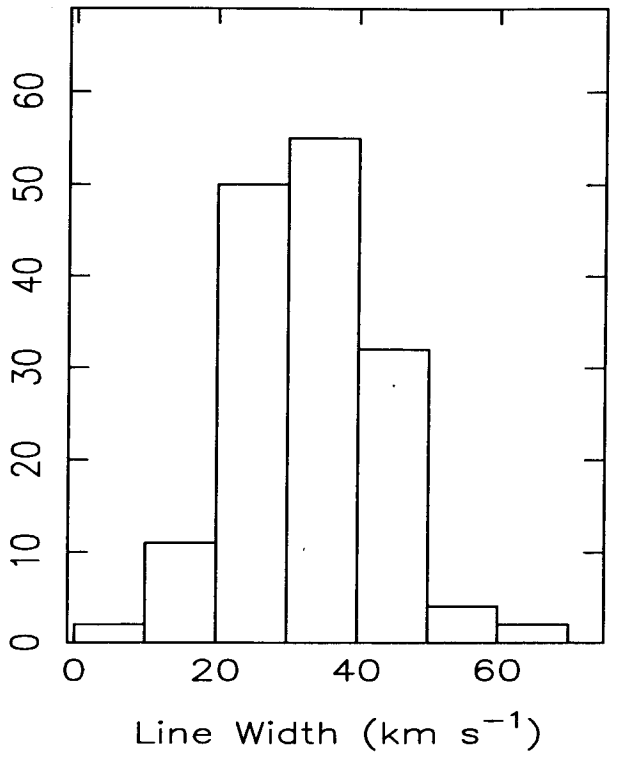

Figure 16. A histogram of the widths of hydrogen recombination lines near 327 MHz detected in the observations with a resolution of $2° \times 6'$.

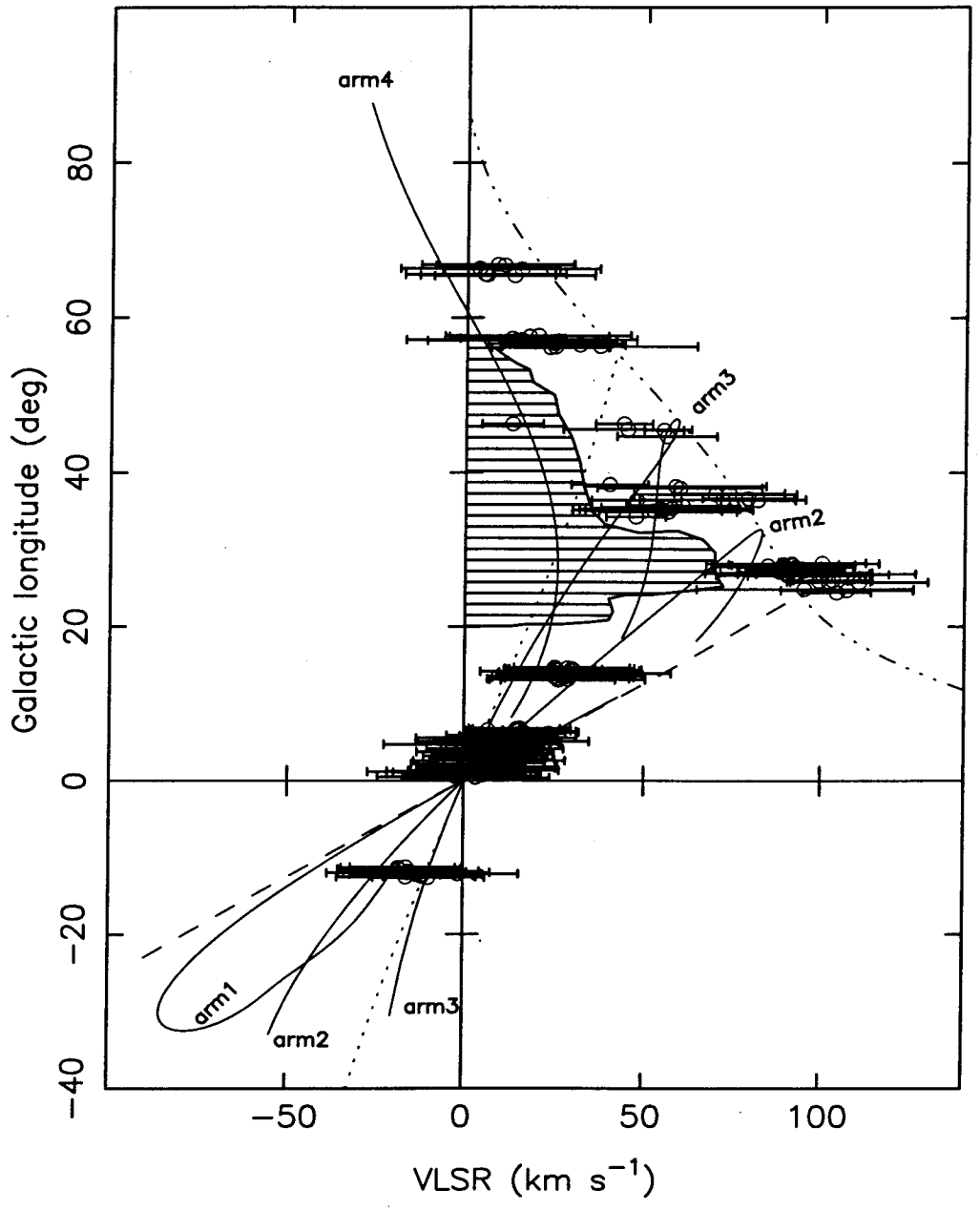

Figure 17. An *l-v* diagram obtained from the hydrogen line emission observed with the 2° × 6′ beam. The open circles represent the central velocity and the horizontal lines indicates the line width. The delineations (solid line) correspond to the four spiral arms (1 to 4 as designated by Taylor & Cordes 1993), the *l-v* diagram corresponding to an annulus of 3.5 kpc (dashed line) and 7 kpc (dotted line) and the terminal velocity at different galactic longitude (dash-dot-dot-dot line). Parameters of galactic rotation given by Burton & Gordon (1978) after scaling them to conform with $R_\odot$ = 8.5 kpc and θ_0 = 220 km s^{-1} are used to get these curves. The striped region corresponds to a region devoid of line emission near 327 MHz as observed in the 2° × 2° survey of Roshi & Anantharamaiah (2000).

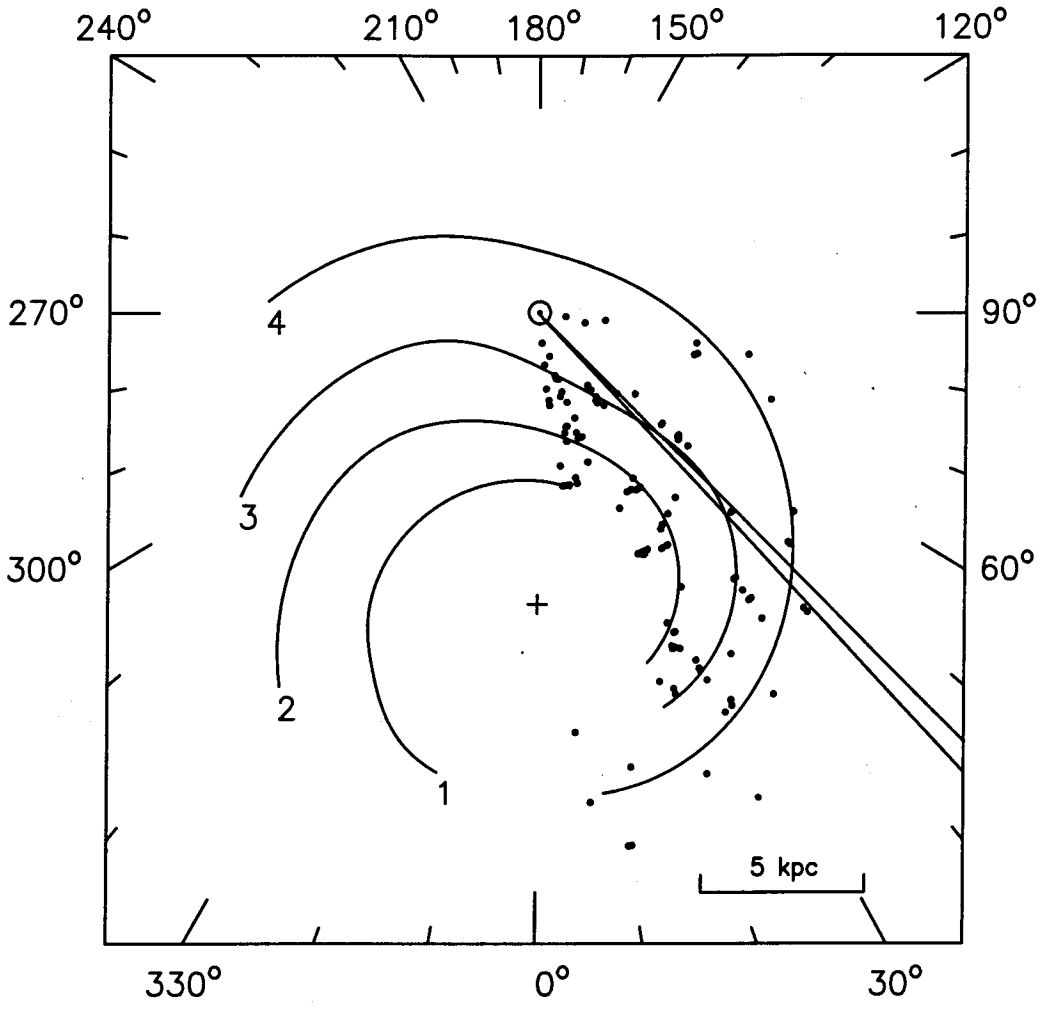

Figure 18. The line of sight through the galactic disk at $l = 45°.5$. The four spiral arms (curved solid lines) and the H II regions (dots) with known distances in the first quadrant are also marked.

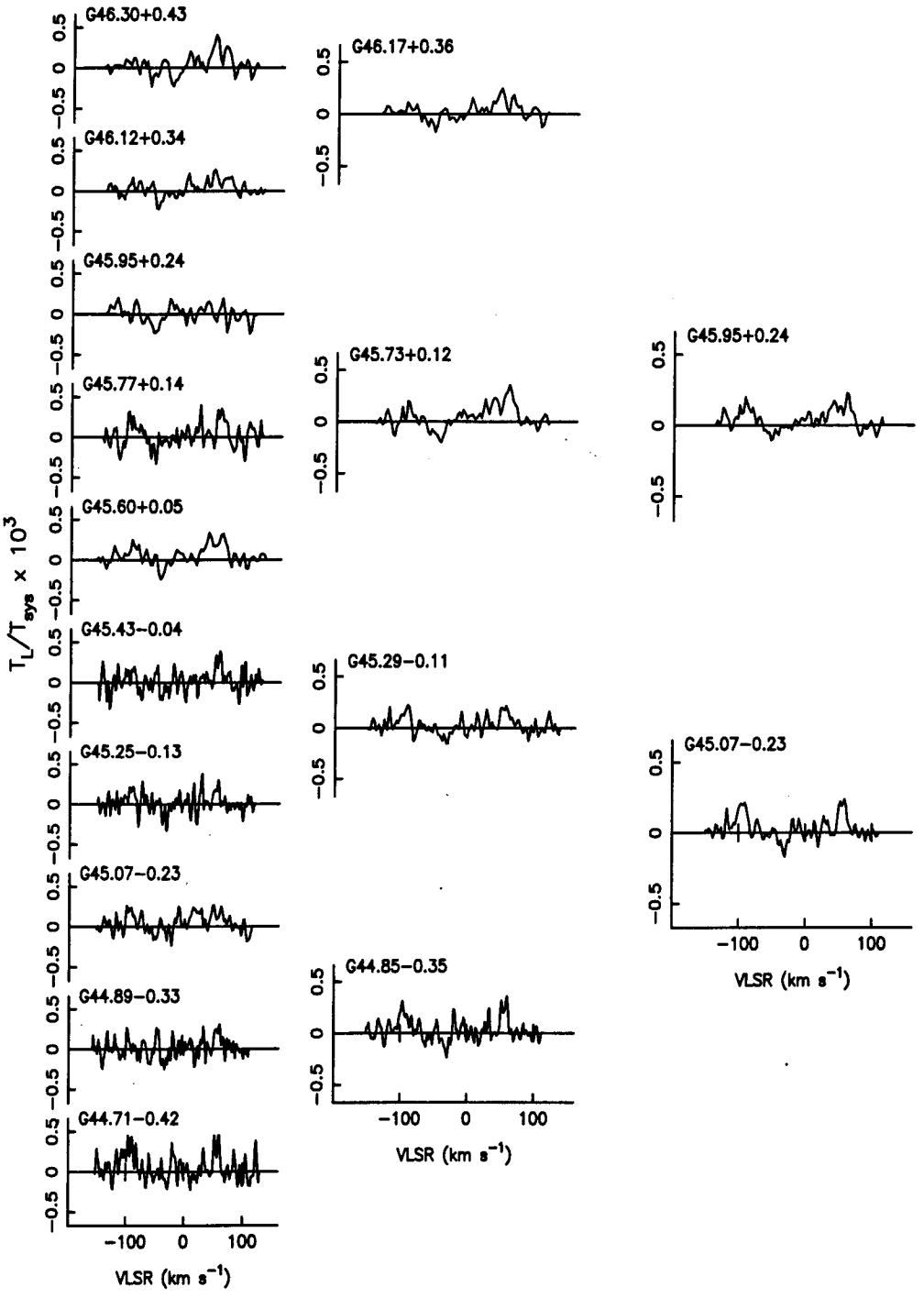

Figure 19. Spectra obtained by averaging different subsets of spectra observed towards field 7 (G45.5+0.0). The spectra shown in the left, center and right column are obtained by averaging over 2° × 12′, 2° × 30′ and 2° × 1° area respectively. The galactic coordinates of the centers of these angular region are shown on the spectra.

References

Anantharamaiah K. R., 1985a, *JAA*, **6**, 177.
Anantharamaiah K. R., 1985b, *JAA*, **6**, 203.
Anantharamaiah K. R., 1986, *JAA*, **7**, 131.
Burton W. B., Gordon M. A., 1978, *A&A*, **63**, 7.
Caswell J. L., Haynes R. F., 1987, *A&A*, **171**, 261.
Cersosimo J. C., 1990, *ApJ*, **349**, 67.
Downes D., Wilson T. L., Bieging J., Wink J., 1980, *A&AS*, **40**, 379.
Erickson W. C., McConnell D., Anantharamaiah K. R., 1995, *ApJ*, **454**, 125.
Gordon M. A., Cato T., 1972, *ApJ*, **176**, 587.
Gottesman S. T., Gordon M. A., 1970, *ApJ*, **162**, L93.
Hart L., Pedlar A., 1976, *MNRAS*, **176**, 547.
Heiles C., 1994, *ApJ*, **436**, 720.
Heiles C., Reach W. T., Koo B.-C., 1996, *ApJ*, **466**, 191
Kantharia N. G., Anantharamaiah K. R., 2001, (this issue).
Konovalenko A. A., Sodin L. G., 1980, *Nat*, **283**, 360.
Lockman F. J., 1976, *ApJ*, **209**, 429.
Lockman F. J., 1980, in Shaver P. A., eds, Radio Recombination Lines, D. Reidel, Dordrecht, p. 185.
Lockman F. J., 1989, *ApJSS*, **71**, 469.
Lockman F., J., Pisano D., J., Howards G., J., 1996, *ApJ*, **472**, 173.
Matthews H. E., Pedlar A., Davies R. D. 1973, *MNRAS*, **165**, 149.
Mezger P. G., 1978, *A&A*, **70**, 565
Payne H. E., Anantharamaiah K. R., Erickson W. C., 1989, *ApJ*, **341**, 890.
Petuchowski S. J., Bennett C. L., 1993, *ApJ*, **405**, 591.
Reich W., Fürst E., Reich P., Reif K., 1990, *A&AS*, **85**, 633.
Roshi A. D., Anantharamaiah K. R., 2000a, 2000, *ApJ*, **535**, 231.
Roshi A. D., Anantharamaiah K. R., 2001, *ApJ* (submitted).
Shaver P. A., 1975, *Pramana*, **5**, 1.
Shaver P. A., 1976, *A&A*, **49**, 1.
Swarup G., *et al.*, 1971, *Nat. Phy. Sci.*, **230**, 185.
Taylor J., H., Cordes J., M., 1993, *ApJ*, **411**, 674.
Wood D. O. S., Churchwell E., 1989, *ApJS*, **69**, 831.